Gondwana Research 28 (2015) 209–224

Contents lists available at ScienceDirect

Gondwana Research

journal homepage: www.elsevier.com/locate/gr

The nature and history of the Qilian Block in the context of the development of the Greater Tibetan Plateau

Hui Huang [a,b,*], Yaoling Niu [a,b,c,*], Geoff Nowell [a], Zhidan Zhao [b], Xuehui Yu [b], Xuanxue Mo [b]

[a] Department of Earth Sciences, Durham University, Durham DH1 3LE, UK
[b] School of Earth Science and Mineral Resources, China University of Geosciences, Beijing 100083, China
[c] Institute of Oceanology, Chinese Academy of Sciences, Qingdao 266071, China

ARTICLE INFO

Article history:
Received 21 July 2013
Received in revised form 17 February 2014
Accepted 24 February 2014
Available online 21 March 2014

Handling Editor: Z.M. Zhang

Keywords:
Syn-collisional magmatism
I-, S-type granitoids
Crust growth
The Qilian Block
The Qilian Ocean

ABSTRACT

The Palaeozoic granitoids in the Qilian Block are important for understanding the tectonic evolution of the Northern Tibetan Plateau. We choose granitoids from Huangyuan (HY) and Gangcha (Gcha) for a detailed study. The granitoids are S-type and I-type, and record different magmatisms from the Neoproterozoic to the Palaeozoic. Most samples have an emplacement age of ~450 Ma with three samples being significantly older (924 Ma, 797 Ma and 503 Ma). The ~924 Ma and ~797 Ma magmatisms represent crustal growth and crustal reworking, respectively. The 503 Ma plagiogranite-like granite carries mantle isotope signatures and resulted from extensive fractional crystallization of mantle-derived melt in a back-arc setting. The ~450 Ma granitoids have various chemical compositions, but most of them share similar trace element patterns resembling the bulk continental crust composition. Despite their large compositional and age variations, significant correlations on SiO_2-variation diagrams and in isotope spaces suggest that these granitoids are different products essentially derived from common sources. The significant mantle contributions (70%–80%, apart from QL09-02) required by whole rock Sr–Nd–Pb–Hf isotopic compositions strongly suggest the "mantle source" as last fragments of the subducted/underthrusting oceanic crust at the onset of collision. Based on all the petrology, geochronology, geochemical data and adjacent tectonic associations, we suggest that the Qilian Ocean started opening in the Neoproterozoic between the Qaidam Block and the Qilian Block. A back-arc basin was developed between the Qilian Block and the Alashan Block shortly after. The 450 Ma granitoids are the products in response to the closure of the Qilian Ocean and the onset of the Qilian–Qaidam continental collision.

1. Introduction

The Greater Tibetan Plateau is a unique architecture that has attracted attention and immense effort of scientists over past decades to understand its origin and evolution as well as its global climatic and environmental impact. It is a giant geological amalgamation made up of micro-continental blocks/slivers, formed as a result of several continental collisions from northeast in the Early Palaeozoic progressively younger towards southwest in the Cenozoic. The youngest India–Asia collision at ~55 Ma and the associated geology and terranes are much better studied, but the earlier events and geology to the north are not, especially, the earliest Qilian–Qaidam system at the northern margin of the plateau.

The Qilian Orogenic Belt (QOB) (Fig. 1A) within the Qilian–Qaidam system at the northernmost margin of the Greater Tibetan Plateau has recorded the histories of continental breakup, seafloor spreading, and the ultimate continental collision from the Neoproterozoic to the Palaeozoic (Song et al., 2009, 2013, 2014). The tectonic subdivision of QOB has evolved over the years, and the most recent suggestion is as follows (Song et al., 2006, 2013, 2014) (Fig. 1A): (1) the north Qilian orogenic belt (NQOB), (2) the Qilian Block (QB), (3) the North Qaidam ultrahigh-pressure metamorphic (NQ-UHPM) belt, and (4) the Qaidam Block (QDB). The metamorphic history has been well studied and reviewed by Song et al. (2013), while the mechanism of continental growth remains unclear. Several models of Qilian Orogenic Belt have been proposed (Xu et al., 1994; Yin and Harrison, 2000; Yang et al., 2002; Gehrels et al., 2003; C.L. Wu et al., 2006; Song et al., 2006; Xiao et al., 2009; Wu et al., 2010; Gehrels et al., 2011; Song et al., 2013, 2014). These models are debating on the location of the suture zone and subduction polarity of the Palaeo-Qilian Oceanic lithosphere. However, the major hindrance is the lack of adequate knowledge of magmatism during the subduction/collision period and therefore the poor time constraints on the onset of subduction and collision. In contrast to the popular

* Corresponding authors at: Department of Earth Sciences, Durham University, Durham DH1 3LE, UK.
E-mail addresses: hui.huang@durham.ac.uk (H. Huang), yaoling.niu@foxmail.com (Y. Niu).

http://dx.doi.org/10.1016/j.gr.2014.02.010
1342-937X/

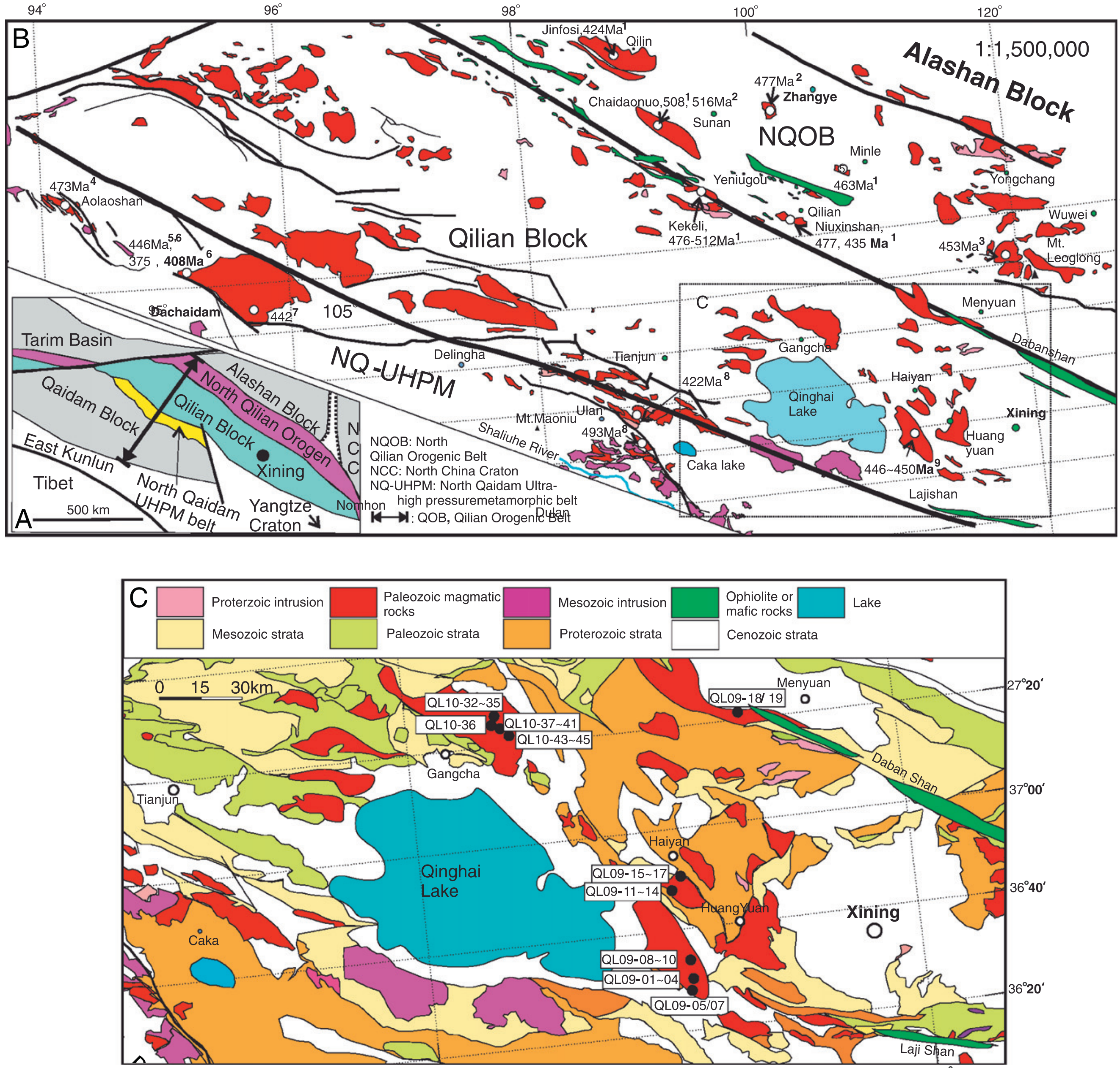

Fig. 1. (A) Schematic map showing major tectonic units of the Qilian Orogenic Belt (after Song et al., 2013). (B) Simplified geological map of the Qilian Block showing the distribution of granitoids and ophiolites (after Pan et al., 2004). Data are from the literature given in Table 1. (C) Detailed geological map of the sampling locations (after Pan et al., 2004).

research of metamorphic rocks within the NQOB and the NQ-UHPM and numerous studies of magmatism within the NQOB, little is known about those granitoids which are coeval with metamorphism at the early Palaeozoic in the QB. Sandwiched between two important tectonic units, the QB is particularly important for understanding the relationship of these subunits and the tectonic histories of the block itself and the region in the context of the Greater Tibetan Plateau evolution.

In this study, we aim to understand the nature of the Qilian Block by studying the petrology, geochronology and geochemistry of the Palaeozoic granitoids with the result also having shed lights on the evolution histories of its sutures to the north (i.e., the NQOB with seafloor subduction-zone complex) and to the south (i.e., the NQ-UHPM separating the Qaidam Block to the south).

2. Tectonic setting and geology background

2.1. Strata, metamorphic rocks and mafic rocks in the QOB

The QOB is a broad and composite orogenic belt bounded by the Yangtze Craton to the southeast, East Kunlun orogenic belt to the south, Alashan Block to the northeast and Tarim Basin to the northwest (Fig. 1A). It has four subunits from the North to South: NQOB, QB, NQ-UHPM and QDB (Fig. 1A).

The NQOB is covered by Carboniferous to Triassic sedimentary sequences. The magmatic clasts within the Silurian flysch formations are dated at 515–429 Ma (Song et al., 2013). The Devonian molasses are also found in this belt. The NQOB is characterized by the occurrence of low-T/HP blueschist and eclogite-facies rocks (Zheng, et al., 2013). The metamorphic rocks record a cold oceanic subduction zone with a thermal gradient of ~6–7 °C/km (Song et al., 2007; Zhang et al., 2007). There are two ophiolite belts in the NQOB (Song et al., 2013). Magmatic zircon dating for ophiolites gives ages varying from 496 to 550 Ma (Song et al., 2013) in the south and from 448 to 490 Ma in the north (Xia and Song, 2010; Song et al., 2013).

The QB, bounded by the NQOB to the north and the NQ-UHPM belt to the south is dominantly Precambrian basement (Chen et al., 2007a; D. Chen et al., 2009; N. Chen et al., 2009) covered with the Palaeozoic sedimentary lithologies. Granitic intrusions with ages of 880–940 Ma as well as the coeval metamorphism are documented (Guo et al., 1999; Tung et al., 2007a, 2007b; Xu et al., 2007; Song et al., 2012, 2013). The Dabanshan ophiolite at the NQOB-QB boundary (Fig. 1B) mainly outcrops as dismembered lenses, consisting of pillow basalt, gabbro, harzburgite, pyroxenite and hornblendite etc. with minor felsic lithologies. Sm–Nd isochron gives the age of ~492 ± 22.6 Ma for basalt (Qinghai Geological Survey Institute, 2006). A few low-K_2O (0.05–0.96 wt.%) tholeiitic dikes cut through the Palaeoproterozoic basement (Qinghai Geological Survey Institute, 2006). The Lajishan ophiolite associating with tonalite, diorite and plagiogranite in the southern QB near the QB and NQ-UHPM boundary (Fig. 1B) is of MORB protolith and dated at 510 Ma (Hou et al., 2005).

The NQ-UHPM belt is characterized by UHPM eclogite-facies blocks and lenses hosted in the UHPM granitic gneisses (Song et al., 2003a, 2003b, 2006; Zhang et al., 2006). The protoliths of the UHPM rocks vary, including granitic gneiss of ~1200–900 Ma and ultramafic rocks of 550–500 Ma (Song et al., 2013; and references therein) and ~877–750 Ma (Yang et al., 2006; Zhang et al., 2011). Previous studies indicate that the HP–UHP metamorphism and subsequent exhumation happened from 497 Ma to 400 Ma (Yang et al., 2002; Song et al., 2003b, 2005, 2006; D. Chen et al., 2009; N. Chen et al., 2009). Volcanic arc basalts of 514 Ma are regarded as reflecting seafloor subduction (Shi et al., 2004).

The QDB is dominated by the Precambrian meta-crystalline basement (Chen et al., 2011) covered with Palaeozoic–Mesozoic sedimentary rocks. It is located to the northwest of the numerous East Kunlun batholiths of Palaeozoic to Mesozoic ages (Chen et al., 2011; Huang et al., 2014).

2.2. Palaeozoic granitoids in the QOB

The Palaeozoic granitoids in the QOB are concisely summarized in Fig. 1B and Table 1. Generally, I-type rocks (453–512 Ma) predate S-type rocks (424–516 Ma) despite some ages overlap (Table 1). They have been interpreted as products in response to varying stages of earlier southward subduction of the Qilian Ocean seafloor underneath the NQOB and later northward subduction underneath the Alashan Block, i.e., the double subduction model (C.L. Wu et al., 2006; Wu et al., 2010) compared to the northward subduction model (Xu et al., 1994; Yin and Harrison, 2000; Song et al., 2013, 2014) and southward subduction model (Gehrels et al., 2003).

Table 1
Compilation of Palaeozoic granitoids in the Qilian Orogenic Belt (QOB).

	Location	Age	Rock-type	Refs.	
NQOB	Kekeli	476–512	I	1	(Wu et al., 2010)
	Kekeli	501	I	1	
	Chaidanuo	508	S	1	
	Niuxinshan	477	I	1	
		435	S	1	
	Minle	463	I,S	1	
	Jinfosi	424	S	1	
	Chaidanuo	516	S	2	(Song et al., 2012)
	Leigongshan	453	I	3	(Tseng et al., 2009)
NQ-UHPM	Aolaoshan	473	I	4	(Wu et al., 2001)
	Dachaidam	446	S	5	(Wu et al., 2002)
	Dachaidam	446	S	6	(Wu et al., 2007)
		408	S	6	
		460–470	I	6	
		370	S	6	
	Dachaidam	442	?	7	(Gehrels et al., 2003)
	Ulan	493	I	8	(Chen et al., 2011)
	Ulan	422	S	8	
QB	Huangyuan	450–446	S	9	(Yong et al., 2008)

Numbers refer to the numbers in Fig. 1B.

There has been only one study on the Palaeozoic batholiths in the QB (Yong et al., 2008). It is a typical S-type batholith of ~446–450 Ma in the Huangyuan (HY) area in the eastern part of the QB (Table 1, Fig. 1B) with $\varepsilon_{Nd}(t)$ of −5.2 and −6.6 (Yong et al., 2008). It is interpreted as derived from metagreywacke in a syncollisional setting without giving details (Yong et al., 2008).

Granitoids in the NQ-UHPM are generally I-type before 446 Ma and S-type after 446 Ma (Fig. 1B, Table 1). The I-type granitoids are interpreted as subduction related and S-type rocks are interpreted as collision related (Wu et al., 2001, 2002; Gehrels et al., 2003; Wu et al., 2007) based on their geochronology and petrology. Chen et al. (2011) report one I-type sample of 493 Ma and two S-type samples of 422 Ma in the Ulan area (Fig. 1B) and propose that they might have a source related to EM II based on the Sr–Nd–Pb–O isotopes, which cannot be justified.

Our samples are collected from 13 locations of several intrusions, generally representative of those in the eastern part of the Qilian Block. GPS data are given in Table 2. Two samples QL09-18 and QL09-19 are from an ophiolite in the Dabanshan at the boundary with the NQOB in the north (Fig. 1B, C, Table 1). Other samples with 'QL09' initials are from Huangyuan (HY) (Table 2) where Proterozoic sedimentary rocks dominate with some Mesozoic strata (Fig. 1C). Samples with 'QL10' initials are from the Gangcha area (Gcha) (Table 2) where Palaeozoic and Mesozoic sedimentary strata dominate (Fig. 1C).

3. Methods

All the 24 samples were analysed for bulk-rock major and trace element compositions at Tianjin Institute of Geology and Mineral Resources, China (See Huang et al., 2014). Nine representative samples were selected for zircon U–Pb dating at China University of Geosciences (Wuhan) following Liu et al. (2008) and China University of Geosciences (Beijing) following Song et al. (2010a). Results from both labs are consistent. The dated samples were analysed for bulk-rock Sr–Nd–Pb–Hf isotopes at the Northern Centre for Isotopic and Elemental Tracing (NCIET) at Durham University. The long term performance of the Neptune in Durham for Sr, Nd and Hf isotopes was reported by Nowell et al. (2003). All the analytical details are given by Huang et al. (2014).

4. Petrology, zircon dating and geochemistry

Samples can be divided into three groups according to their ages, mineralogy, and geochemical compositions (Table 1). Three samples are significantly older than others: 924 Ma, 797 Ma and 503 Ma, respectively. Other samples are ~450 Ma I-type granitoids with no Al-rich minerals and S-type granitoids containing Al-rich minerals, e.g. garnet (Grt), muscovite (Ms) and allanite (Aln) (Table 1, Fig. 2). Bulk-rock major and trace element data are given in Table 3, and Sr–Nd–Pb–Hf isotope data are given in Table 4. They are all calc-alkaline (Fig. 3) and define good correlations on SiO_2-variation diagrams (Fig. 4).

4.1. Old rocks—924 Ma, 797 Ma and 503 Ma

Granite QL09-15 is slightly deformed, containing Qz, Pl, Kfs, and Ms. It has enriched light rare earth element (LREE) patterns with flat heavy REEs (HREEs) (Fig. 5). Zircons are weak luminescent and well oscillatory zoned (Fig. 6) with high Th/U ratios (0.18–0.49, Table S1). Twenty one analyses give a coherent concordant $^{206}Pb/^{238}U$ age of 924.1 ± 1.5 Ma (Fig. 7), representing the crystallization age. The inherited zircons

Table 2
Sample locations and brief descriptions of the studied samples in the Qilian Block.

	Sample	Age	GPS position		Mineral assemblage	SiO_2%	A/CNK
Old rocks	QL09-15	924	N36°48.726′	E101°09.977′	Pl, Kfs, Grt, Ms, Qz, slightly deformed	70.0	1.17
	QL09-01	797	N36°27.116′	E101°05.634′	Qz, Kfs, Pl, Bt, Ms, Grt	72.7	1.31
	QL09-18	503	N37°22.712′	E101°23.887′	Qz, Pl, Chl, minor Kfs, slightly deformed	72.3	1.23
	QL09-19		N37°22.712′	E101°23.887′	Amp, Pl	51.6	0.79
S-type	QL09-02	430	N36°27.116′	E101°05.634′	Qz, Kfs, Pl, Bt, Ms	72.4	1.17
	QL09-07		N36°27.047′	E101°05.557′	Qz, Kfs, Pl, Chl, calcite vein	71.9	1.66
	QL09-09		N36°34.895′	E101°13.520′	Qz, Kfs, Pl, Bt, Ms	70.8	1.06
	QL09-10	430	N36°34.895′	E101°13.520′	Qz, Pl, Bt, Ms, Grt	75.1	1.05
	QL09-12	430	N36°46.731′	E101°07.428′	Qz, Kfs, Pl, Bt, Aln	71.3	1.10
	QL09-17		N36°48.672′	E101°09.914′	Qz, Kfs, Pl, Bt, Ms	69.6	1.17
	QL10-40 F		N37°23.678′	E100°27.800′	Minor Bt, Ms, Q, altered feldspar, *F*	74.8	1.10
	QL10-41 F		N37°23.678′	E100°27.800′	Similar to QL10-40(*F*), thermol equiliabrated with QL10-41(*C*) in the thin section, *F*	74.8	1.15
I-type	QL09-14	450	N36°46.903′	E101°07.562′	Qz, Pl, Amp > Bt, *F*	56.0	0.79
	QL10-32		N37°25.962′	E100°27.615′	Bt, Pl, Qz, Amp, Chl, *F*	62.0	0.94
	QL10-33		N37°25.962′	E100°27.615′	Bt, Amp, Pl, Qz, *F*	62.2	0.95
	QL10-34	450	N37°25.962′	E100°27.615′	Bt, Amp, Pl, Qz, *F*	62.1	0.92
	QL10-35		N37°25.962′	E100°27.615′	Bt, Amp, Pl, Qz, *F*	61.7	0.90
	QL10-44		N37°23.678′	E100°27.800′	Bt, Amp, Pl, Qz, *F*	60.2	0.96
	QL10-45		N37°23.678′	E100°27.800′	Bt, Amp, Pl, Qz, *F*	62.4	1.00
	QL10-37	450	N37°23.678′	E100°27.800′	Bt, Qz, Pl, *C*	74.1	1.05
	QL10-38		N37°23.678′	E100°27.800′	Bt, Qz, Pl, more Bt and Pl, *C*	62.1	1.08
	QL10-40C		N37°23.678′	E100°27.800′	Bt, Qz, Pl, *C*	69.3	1.11
	QL10-41C		N37°23.678′	E100°27.800′	Bt, Qz, Pl, *C*	67.9	1.12
	QL10-42		N37°22.629′	E100°28.641′	Bt, Qz, Pl, *C*	65.0	1.11

Pl: plagioclase; Kfs: K-feldspar; Grt: garnet; Ms: muscovite; Qz: quartz; Bt: biotite; Amp: amphibole; Chl: chlorite; Aln: allanite.
F: fine-grained; *C*: coarse-grained.
Mineral abbreviations follow Whitney and Evans (2010).

> 1.0 Ga are discordant and fail to form a Discordia line (Fig. 7), but these data indicate the presence of ancient crystalline rocks in the QB. The slightly negative $\varepsilon_{Nd}(924)$ value (−3.8) (Table 4) indicates crustal contributions demonstrated by inherited old zircons in this sample (Fig. 7). The whole-rock $\varepsilon_{Hf}(924)$ value of up to 3.8 (Table 4) emphasizes the significant mantle input.

Granite QL09-01 consists of Qz, Kfs, Pl, Bt, Grt and Ms with partial melting texture (sieved texture, broken down minerals, vesicles, and small percentage of brown glass along grain boundary) (Fig. 2A). It has an enriched LREE pattern with flat HREEs (Fig. 5). Zircon populations are complex in this sample with Th/U ratios varying from 0.23 to 1.55 (Table S1). Some of them display sector zoning, strip zoning, homogeneous in oval shape or clear core–mantle structure (Fig. 6). These grains form a Discordia line with an Archaean upper intercept of 2769 Ma (Fig. 6). Other grains are prismatic with oscillatory zoning (Fig. 6) and form two populations (Fig. 7): concordant Palaeoproterozoic age of ~1800 Ma (blue points of QL09-01 in Fig. 7) and Neoproterozoic concordant age of 796.7 Ma (Fig. 7). Both

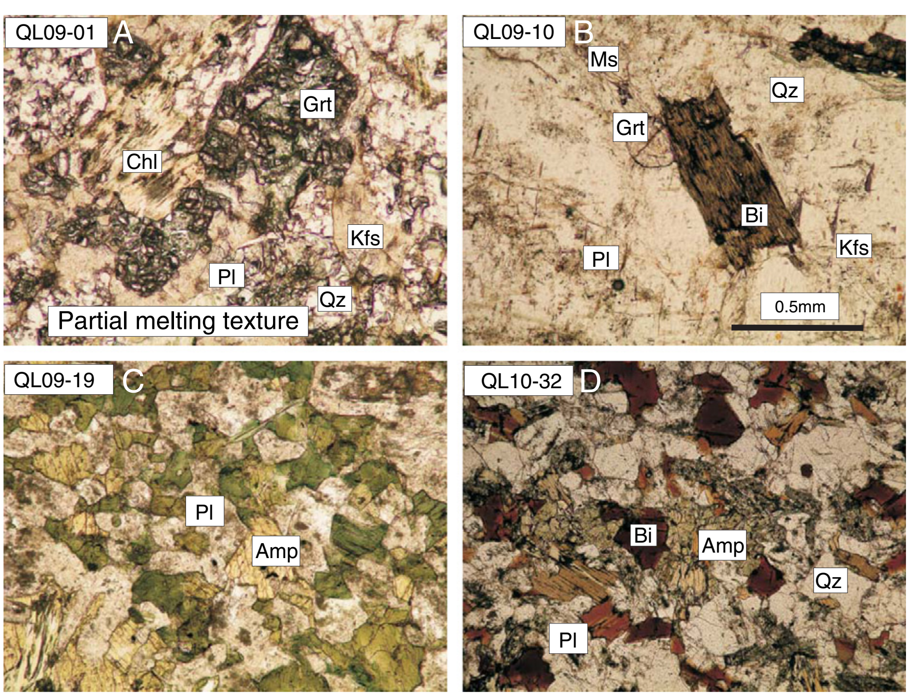

Fig. 2. Photomicrographs under plane polarized light showing partial melting textures of QL09-01 (A), representative S-type granite QL09-10 (B), enclave QL09-19 in QL09-18 (C) and I-type granite QL10-32 (D).

Table 3
Bulk rock major and trace element data of granitoids in the Qilian Block.

	Old rocks				450 Ma S-type							
	QL09-15	QL09-01	QL09-18	QL09-19	QL09-02	QL09-07	QL09-09	QL09-10	QL09-12	QL09-17	QL10-40 F	QL10-41 F
SiO_2	70.0	72.7	72.3	51.6	72.4	71.9	70.8	75.1	71.3	69.6	74.8	74.8
TiO_2	0.28	0.52	0.36	0.72	0.22	0.75	0.32	0.07	0.24	0.31	0.06	0.07
Al_2O_3	15.5	12.3	14.3	17.4	14.6	11.7	14.9	13.4	14.8	15.8	13.9	14.1
Fe_2O_3	1.19	1.14	0.96	3.61	0.46	1.40	0.69	0.35	0.87	0.98	0.32	0.41
FeO	1.32	2.40	1.97	6.05	0.75	4.00	1.76	0.60	0.90	1.87	0.50	0.45
FeO_T	2.39	3.43	2.83	9.30	1.16	5.26	2.38	0.91	1.68	2.75	0.79	0.82
MnO	0.04	0.07	0.05	0.19	0.02	0.11	0.06	0.07	0.04	0.05	0.03	0.03
MgO	0.59	1.46	1.05	4.76	0.50	2.31	0.66	0.19	0.76	0.63	0.17	0.17
CaO	1.85	1.31	1.18	8.19	0.86	1.07	2.21	1.11	1.66	2.05	0.56	0.53
Na_2O	3.23	2.48	5.11	1.27	2.40	2.03	3.44	3.14	3.44	3.30	3.70	3.66
K_2O	4.23	2.67	0.97	3.53	6.44	1.63	3.98	5.16	4.45	4.01	5.14	4.86
P_2O_5	0.09	0.06	0.08	0.15	0.11	0.09	0.13	0.02	0.10	0.09	0.09	0.10
LOI	1.41	2.43	1.35	1.73	1.05	2.50	0.73	0.50	1.14	0.96	0.55	0.53
Total	98.3	97.1	98.3	97.5	98.8	97.0	98.9	99.2	98.6	98.7	99.3	99.2
A/CNK	1.17	1.31	1.23	0.79	1.17	1.66	1.06	1.05	1.10	1.17	1.10	1.15
Li	55.8	25.8	4.39	5.61	9.94	21.9	76.0	32.0	54.7	56.9	12.9	13.9
Sc	5.36	8.60	7.76	33.7	2.80	6.61	5.22	1.81	4.51	7.59	2.79	2.29
Cr	9.18	47.3	2.90	16.3	19.9	16.0	3.89	1.16	16.2	10.9	5.02	5.55
Co	3.81	7.3	2.20	24.5	2.0	4.63	2.65	0.44	2.98	5.14	0.68	0.69
Ni	4.02	12.6	2.50	11.9	3.4	12.5	1.66	0.67	2.48	4.84	0.90	1.03
Ga	18.4	16.0	19.0	18.0	13.8	16.6	20.2	13.6	18.3	21.0	18.0	18.0
Rb	138	104	21.3	25.9	177	119	163	175	166	181	245	231
Sr	109	254	208	325	336	181	332	97.3	336	103	24.3	18.6
Y	19.8	17.4	12.5	22.8	5.97	6.86	18.9	25.8	17.2	25.8	20.0	18.9
Zr	144	263	130	26.5	107	100	181	73	137	149	43.5	50.4
Nb	9.1	12.7	8.11	6.06	5.98	10.7	19.0	8.0	13.0	10.8	21.5	25.2
Ba	824	668	366	411	1542	580	870	207	978	616	135	78.0
La	25.8	45.0	14.0	18.2	28.6	25.9	43.9	17.8	32.4	33.1	10.0	9.69
Ce	50.3	78.3	31.3	38.2	54.0	51.2	80.7	31.1	56.7	67.4	18.6	19.0
Pr	6.41	8.95	3.48	5.08	6.46	6.09	9.24	4.11	6.84	8.17	2.59	2.58
Nd	24.6	31.3	13.4	21.4	23.1	22.7	32.5	15.2	24.0	30.6	9.41	9.73
Sm	5.05	5.15	2.73	4.56	4.65	4.87	5.47	3.03	4.34	6.38	2.50	2.66
Eu	1.00	1.17	0.78	1.23	1.57	0.86	1.14	0.40	1.01	0.99	0.20	0.14
Gd	4.37	4.38	2.75	4.04	3.61	3.75	4.32	2.46	3.49	5.40	2.54	2.66
Tb	0.68	0.62	0.44	0.69	0.45	0.45	0.63	0.48	0.55	0.86	0.57	0.58
Dy	3.83	3.39	2.42	4.23	1.77	1.84	3.49	3.77	3.14	4.91	3.69	3.59
Ho	0.76	0.68	0.51	0.89	0.25	0.30	0.70	1.06	0.63	0.95	0.71	0.69
Er	2.08	1.93	1.54	2.48	0.53	0.71	1.99	3.92	1.74	2.59	2.01	1.97
Tm	0.30	0.30	0.28	0.38	0.06	0.09	0.31	0.74	0.27	0.38	0.33	0.32
Yb	1.92	1.91	1.66	2.49	0.38	0.58	2.14	5.49	1.82	2.43	2.25	2.13
Lu	0.29	0.30	0.28	0.37	0.06	0.08	0.34	0.96	0.28	0.36	0.32	0.30
Hf	4.38	6.90	4.16	1.14	3.30	2.86	5.56	2.88	4.30	4.62	2.22	2.51
Ta	0.98	0.74	0.70	0.34	0.65	0.68	1.90	1.13	1.52	1.23	4.21	6.09
Pb	26.6	28.5	3.41	6.82	52.2	22.7	40.2	54.7	42.5	30.3	33.7	27.7
Th	11.7	12.7	5.05	1.86	11.4	11.6	20.9	20.3	17.7	14.3	7.33	7.45
U	1.76	1.57	1.02	0.62	1.21	0.79	7.80	4.90	2.13	2.06	2.37	3.15

	450 Ma I-type											
	QL09-14	QL10-32	QL10-33	QL10-34	QL10-35	QL10-37	QL10-38	QL10-40C	QL10-41C	QL10-42	QL10-44	QL10-45
SiO_2	56.0	62.0	62.2	62.1	61.7	74.1	62.1	69.3	67.9	65.0	60.2	62.4
TiO_2	0.90	0.76	0.76	0.74	0.76	0.27	0.78	0.55	0.66	0.74	0.89	0.81
Al_2O_3	16.4	16.3	16.5	16.2	16.2	13.1	17.4	15.1	15.6	16.2	16.3	16.2
Fe_2O_3	2.44	1.27	0.88	0.90	0.95	0.40	1.26	0.74	0.78	1.17	1.39	1.24
FeO	4.98	3.82	3.92	4.10	4.10	1.42	4.20	2.70	3.31	3.77	5.82	4.96
FeO_T	7.18	4.96	4.71	4.91	4.95	1.78	5.33	3.37	4.01	4.82	7.07	6.08
MnO	0.13	0.09	0.08	0.09	0.09	0.03	0.07	0.04	0.07	0.06	0.15	0.12
MgO	5.12	3.29	3.05	3.34	3.38	0.66	2.08	1.50	1.72	1.92	2.99	2.68
CaO	7.90	5.34	5.12	5.43	5.45	1.64	3.72	2.97	3.38	3.22	4.67	4.24
Na_2O	2.59	3.10	3.12	3.04	3.00	2.46	3.72	3.07	3.36	3.33	3.65	3.51
K_2O	1.88	2.29	2.68	2.55	2.91	5.05	2.90	2.88	2.10	3.00	2.30	2.47
P_2O_5	0.17	0.19	0.23	0.18	0.19	0.22	0.33	0.16	0.19	0.26	0.31	0.28
LOI	0.86	1.01	0.94	0.89	0.84	0.37	0.94	0.68	0.61	0.83	0.65	0.59
Total	98.5	98.5	98.5	98.7	98.7	99.3	98.6	99.0	99.1	98.7	98.7	98.9
A/CNK	0.79	0.94	0.95	0.92	0.90	1.05	1.08	1.11	1.12	1.11	0.05	0.05
Li	16.0	45.8	52.8	43.2	46.8	59.0	114	90.6	124	145	68.9	68.4
Sc	22.7	16.6	13.8	16.6	15.1	5.24	12.5	9.44	9.19	13.5	28.6	14.8
Cr	68.4	59.3	58.0	61.1	61.5	14.7	38.0	28.2	32.2	40.4	83.5	58.0
Co	22.5	15.3	14.4	14.8	15.2	3.60	10.5	7.19	8.80	9.75	13.8	13.0
Ni	12.4	10.8	14.2	10.7	11.4	3.68	9.70	6.85	8.18	8.56	22.2	17.8
Ga	17.9	18.3	19.1	17.8	18.2	15.7	26.6	20.4	21.2	25.9	22.5	21.6
Rb	83.6	124	144	130	141	172	170	153	148	193	145	152
Sr	267	219	214	211	216	214	274	280	286	254	230	264

(continued on next page)

Table 3 (*continued*)

	450 Ma I-type											
	QL09-14	QL10-32	QL10-33	QL10-34	QL10-35	QL10-37	QL10-38	QL10-40C	QL10-41C	QL10-42	QL10-44	QL10-45
Y	26.7	19.6	17.5	22.0	20.2	33.5	38.9	15.5	11.6	32.4	52.7	36.2
Zr	170	191	200	194	199	137	228	194	212	258	232	216
Nb	9.4	12.6	12.4	12.1	12.3	10.4	31.2	14.6	15.2	27.8	20.6	18.8
Ba	413	470	604	470	716	1120	321	821	382	566	267	429
La	24.5	43.5	48.2	34.0	40.4	57.8	18.6	43.2	60.5	62.5	39.5	47.2
Ce	50.5	82.6	87.4	63.2	75.8	113	37.2	78.2	111	121	65.3	82.4
Pr	6.34	9.35	10.2	8.00	8.80	13.6	4.94	9.08	13.0	14.9	10.0	11.4
Nd	24.5	33.4	35.3	30.3	32.1	50.6	19.8	31.5	45.9	55.8	41.2	43.4
Sm	5.10	5.76	5.74	5.70	5.67	10.2	5.3	4.91	6.88	11.0	10.6	9.10
Eu	1.12	1.19	1.28	1.19	1.26	1.38	1.36	1.31	1.32	1.40	1.17	1.28
Gd	4.73	5.09	4.88	5.12	5.1	8.94	5.87	4.06	5.52	9.52	10.6	8.24
Tb	0.82	0.74	0.68	0.79	0.75	1.39	1.22	0.6	0.70	1.41	1.96	1.38
Dy	4.98	3.95	3.57	4.42	4.12	7.53	7.62	3.26	3.09	7.28	11.6	7.77
Ho	1.04	0.74	0.65	0.84	0.77	1.25	1.42	0.58	0.50	1.23	2.11	1.41
Er	2.88	1.99	1.80	2.28	2.06	3.08	3.83	1.54	1.12	3.05	5.41	3.68
Tm	0.42	0.29	0.26	0.33	0.30	0.41	0.54	0.23	0.14	0.41	0.75	0.50
Yb	2.73	1.82	1.70	2.20	1.89	2.50	3.45	1.47	0.96	2.51	4.52	3.09
Lu	0.42	0.27	0.26	0.33	0.30	0.37	0.5	0.23	0.16	0.37	0.62	0.43
Hf	4.44	5.06	5.46	5.65	5.47	4.4	6.72	5.53	6.06	7.73	6.69	6.70
Ta	0.61	0.92	0.92	1.07	0.99	0.93	2.41	1.32	1.40	2.17	1.22	1.46
Pb	8.6	19.7	21.1	20.9	22.6	54.5	25.6	25.9	20.2	32.3	14.3	18.0
Th	7.7	15.40	17.6	13.6	14.2	35.5	7.88	10.9	17.0	33.6	12.8	17.0
U	0.80	1.64	1.82	1.70	1.69	4.15	3.18	2.21	2.21	3.73	2.02	3.19

$\varepsilon_{Nd}(800)$ and $\varepsilon_{Hf}(800)$ are negative (−9.8 and −8.4, respectively, Table 4), indicating a crustal origin with less mantle input.

Granite QL09-18 has high SiO_2 (72.3 wt.%) and Na_2O (5.11 wt.%), low K_2O (0.97 wt.%) and moderate CaO (1.18 wt.%), and is peraluminous (A/CNK: 1.23) (Table 3). Minerals include Qz, Pl and Kfs. Minor chloride occurs along the mineral boundaries and mineral cracks. It has an enriched REE pattern with a weak negative Eu anomaly and slightly upward HREEs (Fig. 5). Zircons are prismatic, oscillatory zoning (Fig. 6) and give a concordant weighted mean $^{206}Pb/^{238}U$ age of 502.9 ± 2.0 Ma (Fig. 7), representing the crystallization age. No inherited zircons are observed in this sample. The enclosed mafic enclave QL09-19 is composed of amphibole and plagioclase (Fig. 2) with 51.6 wt.% SiO_2 (Table 3). It has similar trace element pattern to its host QL09-18 with higher elemental concentrations (Fig. 5A, B). Both QL09-18 and QL09-19 have the same level of Eu anomaly (Eu/Eu* = 0.86, Table 3). QL09-18 carries strong mantle isotopic signature, e.g. highly positive $\varepsilon_{Nd}(503)(3.1)$ and $\varepsilon_{Hf}(503)(16.8)$, is less radiogenic I_{Sr} (0.7062) yet highest Pb isotope ratios ($^{206}Pb/^{204}Pb_i$ = 20.474; $^{207}Pb/^{204}Pb_i$ = 15.731; $^{208}Pb/^{204}Pb_i$ = 39.594) (Fig. 8, Table 4). Its mineralogy and geochemical composition resemble plagiogranite despite the apparent lack of petrotectonic constraints.

4.2. ~450 Ma I-type and S-type

S-type samples (Table 2, Fig. 2) are all highly felsic (SiO_2 > 70.4 wt.%) and peraluminous (A/CNK > 1.17) (Tables 2 and 3), consisting of Qz, Kfs, Pl, Bt and Ms. They have LREE enriched patterns with dominant flat HREEs (Fig. 5C, D). Two-mica granite sample QL09-02 and QL09-07 are characterized by depleted HREEs (Fig. 5C, D), indicating the presence of garnet as a residual phase during melting in the source. Sample QL09-10 has elevated HREEs (Fig. 5C, D). Two fine-grained granites (QL10-40F, QL10-41F, Fig. 5C, D; Table 2) display a 'V' shape REE pattern with low LREE abundances, a pronounced negative Eu anomaly and high abundance of Ta, resembling highly evolved melts.

I-type rocks (Table 2, Fig. 2) are fine- and coarse-grained with gradational contact between each other. Fine grained samples consist of Pl, Qz, Amp and Bt. A/CNK values are ≤1. Coarse-grained samples consist of Pl, Qz and Bt without Amp. They all show similar REE patterns (Fig. 5E, F), resembling the bulk continental crust signature (BCC) (Fig. 5) with negative Eu, Nb–Ta–Ti anomalies, a prominent positive Pb anomaly and a flat HREE pattern.

4.3. Ages of I- and S-type samples

Ages of > 1.0 Ga are given by the zircons with distinct core–mantle structure. Zircons with ages varying from 420 Ma to 510 Ma (Fig. 7) do not have clear differences from each other; they are all magmatic grains showing similar structures under CL images (Fig. 6), i.e., oscillatory zoning, strip zoning or homogenous with Th/U ratios > 0.1 (Table S1). Young and old ages can be either on the rims or on the centre, which rule out the possibility of cryptic core–mantle structure. The scattering concordant ages along Concordia might be common in the S-type granitoids. But the I-type samples in this study also tend to have the similar age distributions as those S-type samples do, which is neither common nor expected. The key observation is that they have large age variations; therefore, it is difficult to obtain reliable weighted mean ages with small MSWD. Theoretically, the youngest clustering group should be the crystallization age for magmatic rocks. For each sample here, zircons younger than 450 Ma are mostly plotted away from the Concordia (at least not as concordant as 450 Ma points) (Fig. 7). Therefore, we interpret 450 Ma as representing the emplacement time, which is consistent with zircon age peaks on the histogram (Fig. 9, $^{206}Pb/^{238}U$ ages with >90% concordance for zircons <1.0 Ga and $^{207}Pb/^{206}Pb$ ages with >85% concordance for zircons >1.0 Ga are plotted). The inherited zircons in these ~450 Ma rocks correspond to the ages of aforementioned older rocks and their inherited zircons. Especially QL09-02 has almost the same inherited zircon distribution as QL09-01(Fig. 7), e.g. Archaean upper intercepts and inherited zircons of ~800 Ma in QL09-02 are coherent with the age of QL09-01.

Granitoids of ~450 Ma have overlapping isotopic compositions with small negative or positive Nd and Hf isotopes (Table 4, Fig. 8). The sample depleted in HREEs (QL09-02/07) has distinct large negative $\varepsilon_{Nd}(450)$ and $\varepsilon_{Hf}(450)$ values (−12 and −12, Table 4), indicating a crustal origin. Importantly, its isotopes are similar to 797 Ma QL09-01

Table 4
Bulk-rock Sr–Nd–Pb–Hf-isotopic data of samples in the Qilian Block. Samples older than ~450 Ma are age corrected to their own crystallization ages and 450 Ma, respectively.

	Old rocks			S-type (450 Ma)				I-type (450 Ma)			
	QL09-15 (924 Ma)	QL09-01 (797 Ma)	QL09-18 (500 Ma)	QL09-02	QL09-10	QL09-12	QL10-40(F)	QL09-14	QL10-34	QL10-37	QL10-40(C)
$^{176}Lu/^{177}Hf$	0.009	0.006	0.01	0.004	0.048	0.01	0.006	0.013	0.008	0.012	0.02
$^{176}Hf/^{177}Hf$	0.282453 (06)[a]	0.282112 (07)[a]	0.283021 (09)[a]	0.282174 (08)[a]	0.282897 (07)[a]	0.282539 (06)[a]	0.282508 (12)[b]	0.282665 (11)[a]	0.282490 (07)[b]	0.282519(07)[b]	0.282715(16)[b]
$\varepsilon_{Hf}(450)$	−4	−15	16	−12	0.1	−1	−0.9	2.6	−2.3	−2.3	2
	3.8 (924 Ma)	−8 (797 Ma)	17 (503 Ma)								
$^{147}Sm/^{144}Nd$	0.1214	0.0979	0.1236	0.1319	0.1214	0.1011	0.0946	0.1214	0.1141	0.1223	0.1612
$^{143}Nd/^{144}Nd$	0.511989 (06)[c]	0.511621 (07)[c]	0.512556 (12)[c]	0.511821 (06)[c]	0.512192 (06)[c]	0.512183 (05)[c]	0.512056 (08)[d]	0.512210 (08)[c]	0.512059 (01)[d]	0.512093(08)[d]	0.512302(15)[d]
$\varepsilon_{Nd}(450)$	−8.3	−14.2	2.6	−12.2	−4.4	−3.4	−5.5	−3.8	−6.6	−6.4	−4.5
	−3.8 (924 Ma)	−9.8 (797 Ma)	3.1 (503 Ma)								
$^{87}Rb/^{86}Sr$	3.61	1.16	0.29	1.49	5.1	1.4	28.56	0.89	1.75	2.28	1.55
$^{87}Sr/^{86}Sr$	0.764464 (11)[e]	0.722690 (12)[e]	0.708230 (13)[e]	0.724259 (09)[e]	0.737846 (12)[e]	0.719163 (09)[e]	0.721548 (10)[f]	0.714467 (11)[e]	0.720432 (09)[f]	0.729853 (09)[f]	0.770567 (15)[f]
$I_{Sr}(450)$	0.74134	0.7153	0.7064	0.7147	0.7051	0.7102	0.5875	0.7088	0.7092	0.7153	0.7606
	0.7169 (924 Ma)	0.7095 (797 Ma)	0.7062 (503 Ma)								
$^{206}Pb/^{204}Pb$	18.561 (1)[g]	17.799 (1)[g]	21.940 (3)[g]	17.671 (1)[g]	19.272 (1)[g]	19.159 (2)[g]	19.054 (1)[h]	18.685 (1)[g]	19.000 (1)[h]	19.199 (1)[h]	19.731 (1)[h]
$^{207}Pb/^{204}Pb$	15.656 (1)[g]	15.589 (1)[g]	15.816 (3)[g]	15.580 (1)[g]	15.693 (1)[g]	15.689 (2)[g]	15.687 (1)[h]	15.652 (1)[g]	15.734 (1)[h]	15.698 (1)[h]	15.753 (1)[h]
$^{208}Pb/^{204}Pb$	38.721 (6)[g]	38.641 (5)[g]	41.924 (10)[g]	38.278 (4)[g]	38.602 (5)[g]	38.967 (6)[g]	39.086 (03)[h]	39.300 (7)[g]	39.268 (04)[h]	40.007 (04)[h]	38.684 (04)[h]
$^{208}Pb/^{204}Pb_i(450)$	38.099	38.011	39.829	37.979	38.088	38.375	38.491	38.043	38.348	39.086	38.377
	37.431 (924 Ma)	37.512 (797 Ma)	39.594 (503 Ma)								
$^{207}Pb/^{204}Pb_i(450)$	15.64	15.576	15.741	15.576	15.670	15.678	15.665	15.624	15.714	15.679	15.735
	15.612 (924 Ma)	15.560 (797 Ma)	15.731 (503 Ma)								
$^{206}Pb/^{204}Pb_i(450)$	18.27	17.56	20.626	17.587	18.873	18.954	18.679	18.197	18.642	18.864	19.422
	17.942 (924 Ma)	17.356 (797 Ma)	20.465 (503 Ma)								

[a] JMC475, 0.282160 ± 08 (2SD, n = 10).
[b] 0.282160 ± 06 (2SD, n = 12). $^{176}Hf/^{177}Hf$ are reported relative to an accepted ratio for JMC475 of 0.282160 (Nowell et al., 1998).
[c] J&M, 0.511110 ± 11 (2SD, n = 19).
[d] 0.511110 ± 07 (2SD, n = 11). $^{143}Nd/^{144}Nd$ are reported relative to an accepted ratio for J&M of 0.511110 (Thirlwall, 1991).
[e] NBS987, 0.710267 ± 10 (2SD, n = 13); 6.
[f] 0.710277 ± 15(2SD, n = 9). $^{87}Sr/^{86}Sr$ are reported relative to an accepted $^{87}Sr/^{86}Sr$ ratio for NBS987 of 0.71024 (Thirlwall, 1991).
[g] NBS981, $^{206}Pb/^{204}Pb$:16.94102 ± 184;$^{207}Pb/^{204}Pb$:15.49811 ± 142;$^{208}Pb/^{204}Pb$:36.71791 ± 512 (2SD, n = 11).
[h] NBS981, $^{206}Pb/^{204}Pb$:16.94083 ± 274;$^{207}Pb/^{204}Pb$:15.49706 ± 115;$^{208}Pb/^{204}Pb$:36.71478 ± 399 (2SD, n = 16).

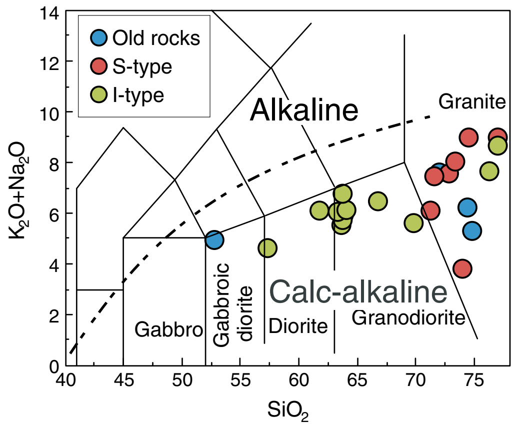

Fig. 3. Total alkalis ($Na_2O + K_2O$) versus SiO_2 (TAS) diagram showing the compositional variation of the QB samples. The dashed line is the division between alkaline and subalkaline fields (Irvine and Baragar, 1971).

(Fig. 8), most likely genetically related. The calculated I_{Sr} for QL10-40F is smaller than 0.700, which is likely an artefact in age-correction due to high Rb/Sr (Han et al., 1997).

5. Discussion

5.1. Origin of 924 Ma and 797 Ma magmatism

Numerous granitoids of ~900 Ma have been reported in the NQOB, QB and NQ-UHPM belts (Guo et al., 1999; Guo and Zhao, 2000; Gehrels et al., 2003; Zhang et al., 2003; Tung et al., 2007a; Song et al., 2012). The 924 Ma QL09-15 is similar to those in the literature (Tung et al., 2008). The small negative zircon $\varepsilon_{Hf}(943)$ (−4.7 to +0.21) (Chen et al., 2007c) and whole rock $\varepsilon_{Nd(943)}$ (−1.38 to −2.84) (Chen et al., 2007b) have led to the interpretation of reworked crust origin (Chen et al., 2007b, 2007c). Our whole rock $\varepsilon_{Hf}(924)$ is up to 3.8. This value is not completely against the previous interpretations but point to a significant juvenile crust component considering the obvious crustal contribution demonstrated by the inherited zircons older than 1.0 Ga (Fig. 7). Therefore, this sample represents a crustal growth event at ~920 Ma; however the exact tectonic setting is hard to conclude based only on one sample.

QL09-01 has high SiO_2 (72.7 wt.%) and Al_2O_3 (A/CNK: 1.31) (Table 3) and negative ε_{Nd} and ε_{Hf} values ($\varepsilon_{Nd}(800)$: −9.8; $\varepsilon_{Hf}(800)$: −8.4, Table 4), implying its dominant reworked lower crustal origin which might be induced by the underplating mantle melt. The observation including inherited zircons (Fig. 7), Discordia with an upper

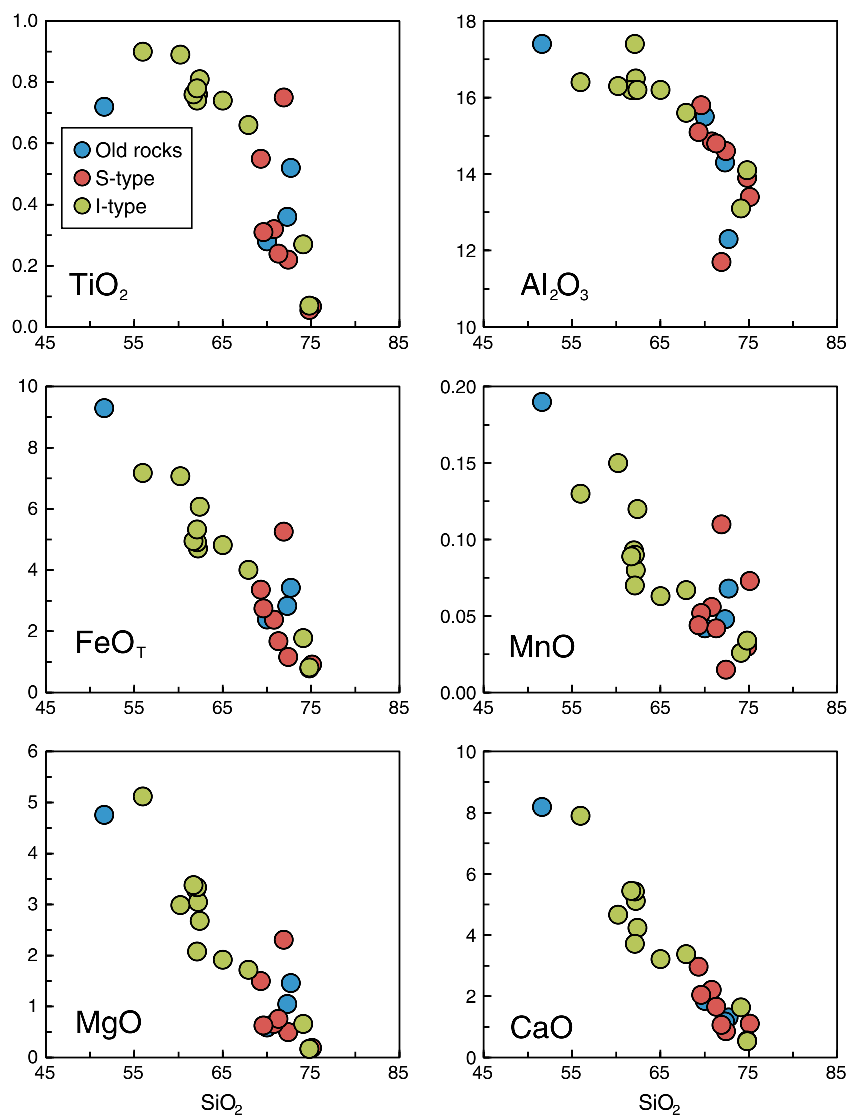

Fig. 4. SiO_2 versus other oxides variation diagrams showing correlated compositional variations among samples.

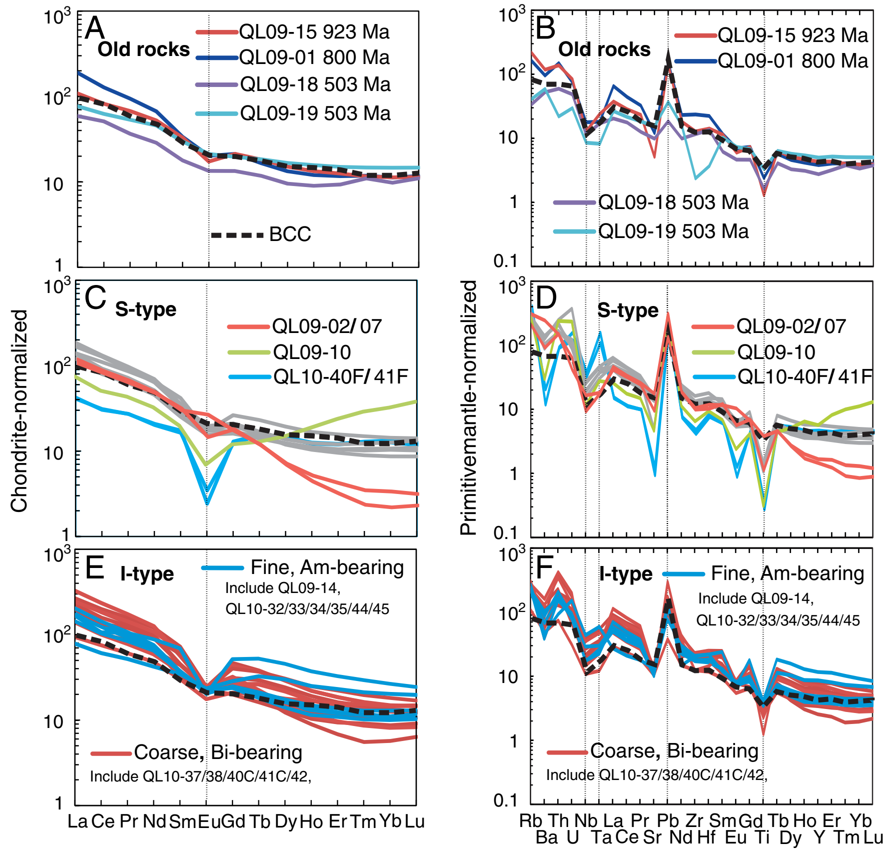

Fig. 5. Chondrite-normalized (Sun and McDonough, 1989) REE patterns for the Qilian Block (QB) samples (left column), and primitive mantle-normalized (Sun and McDonough, 1989) multi-element patterns (right column).

intercept of Archaean age in this study (Fig. 7), and the oldest basement of 2348–2470 Ma found in Qilian Block with Archaean Hf isotope model ages (Chen et al., 2007b; Li et al., 2007) have particular importance that they of the Archaean basement underneath Qilian Block and that Qilian Block must have been a microcontinent during its journey of drift in the ancient ocean and later-on continental collisions.

5.2. Origin of 503 Ma granite

The strong mantle isotopic character of sample QL09-18 (ε_{Nd}(503): 3.1; ε_{Hf}(503): 17, Table 4) is similar to the NQ-UHPM eclogites (Zhang et al, 2008) (Fig. 8), and indicates that it is either directly or indirectly derived from a depleted mantle source. Though there is no direct evidence for QL09-18 as plagiogranite, we suggest the same origin for it, i.e., it was derived from extensive differentiation (up to 80%–90% fractional crystallization) (Spulber and Rutherford, 1983; Floyd et al., 1998) from a low-K tholeiitic magma under hydrous conditions which is a widely used model for the petrogenesis of plagiogranite (Kay and Senechal, 1976; Flagler and Spray, 1991; Rollinson, 2009). Using the simple batch melting model, the original mantle source can be varied from slightly depleted to slightly enriched in LREEs, depending on the degree of partial melting. The problem is that extensive fractional crystallization could have resulted in the prominent negative Eu anomaly. However, the enclosed mafic diorite enclave QL09-19 representing the earlier cumulate has the identical Eu/Eu* anomaly with QL09-18. This means that fractionation of QL09-19 would have not necessarily resulted in the pronounced negative Eu anomaly in QL09-18.

5.3. Origin of ~450 Ma I-type and S-type granites

5.3.1. 'Mixing process'

The significant correlations on SiO_2-variation diagrams (Fig. 4) and isotope plots (Fig. 8) all point to an apparent 'mixing process' which is further demonstrated by positive correlations between initial Pb isotopic ratio and both ε_{Hf} and ε_{Nd} (Fig. 8). Importantly, ε_{Hf}(t) is negatively correlated with A/CNK (Fig. 8F, except QL09-18), reflecting that the more peraluminous samples have more crustal (vs. mantle) contributions as expected. The old rocks (924 Ma, 797 Ma and 503 Ma) are also plotted on the trend defined by these ~450 Ma granitoids (Fig. 8) (924 Ma sample has relatively radiogenic Sr isotopes probably due to post-magmatic modification process as it is slightly deformed). However, it is physically unlikely that these granitoids of such a wide spatial and temporal variation are derived from mixing two singular melts. The inherited zircons of aforementioned ages, e.g. 924 Ma, 797 Ma and 503 Ma, repeatedly occur in the 450 Ma rocks (Fig. 7). This observation, combined with the linear trends on the isotopes, suggests that these old rocks repeatedly underwent reworking processes with varying proportions of mantle input, in other words, they were essentially derived from the same source at different times.

Simple binary isotopic mixing modelling is used to constrain the source materials (Fig. 8). The mantle endmember is represented by the eclogites in the NQ-UHPM (yellow star in Fig. 8, Zhang et al., 2008) whose protolith is the ocean crust possessing the mantle isotope signatures. Although the Archaean basement is involved, we choose to use Mohe basement of 2348–2470 Ma (Chen et al., 2007b; Li et al., 2007) as crustal component because it is the oldest basement with reliable Hf isotopes and inherited zircons of this age are sampled in this

Fig. 6. Cathodoluminescence (CL) images of zircons from representative samples. Black circles with white outlines are analysed spots. The numerals are ages in Ma.

study. Therefore the mantle contributions herein are underestimated. The modelling requires 70%–80% mantle contributions for most samples (except for samples QL09-02). This is a strong constraint that the mantle cannot be the appropriate source as 70–80% mantle derived basalts would make the final magma basaltic rather than peraluminous granitic composition. Hence, the source candidates should be basaltic or andesitic (thus the derived melt can be andestic or granitic) and carry mantle isotopic signatures. They are possibly (1) the subducted oceanic crust, (2) the newly formed island arc crust; and (3) the continental arcs. The newly formed island arc crust is unlikely as it is not easy to explain how to melt these topographically high level rocks that are too cold (Niu and O'Hara, 2003, 2009) to produce granitoids at depth. The earlier 'I-type' granitoids in the NQ-UHPM (Wu et al., 2001, 2007; Chen et al., 2011) could be the continental arc and it is very likely that they play a

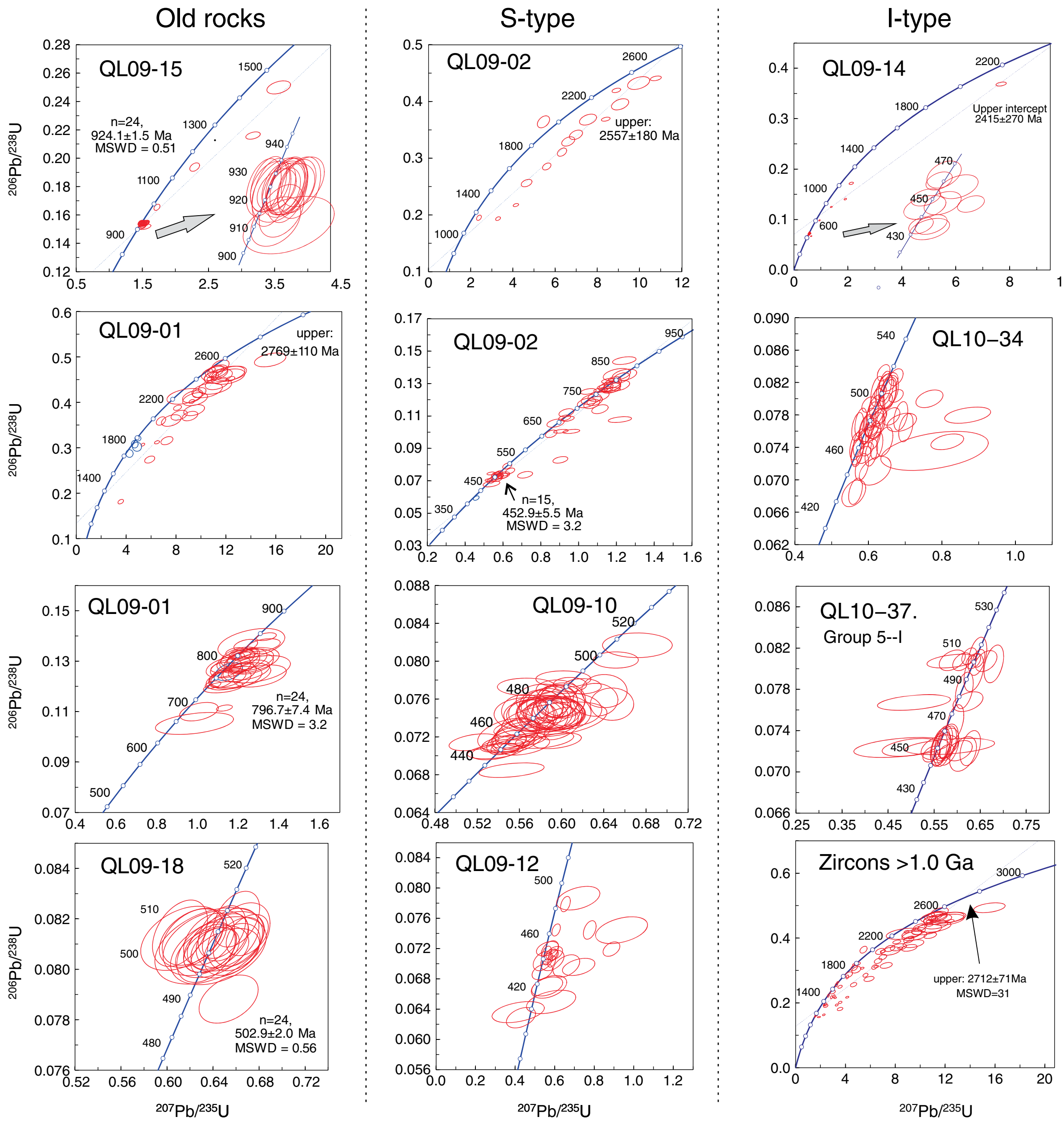

Fig. 7. Zircon U–Pb Concordia diagrams. Old rocks 924 Ma QL09-15, 797 Ma QL09-01 and 503 Ma QL09-18 are well dated. 450 Ma I-type and S-type rocks have large age ranges and are not well dated. We choose the youngest peak at ~450 Ma on the histogram as the emplacing time (see text).

role in the origin of these granitoids evident from the zircons of >450 Ma (Figs. 7 and 9). But continental arc alone cannot explain the large compositional variation of the 450 Ma granitoids and also lack of reliable isotope constraints. Importantly, it requires very limited crustal assimilation to maintain the dominant mantle isotope signature. Considering all the petrology and geochemistry, we suggest that the most suitable candidate is the subducted oceanic crust because (1) its derived melt is andesitic, and (2) it carries mantle isotopic signatures (see Mo et al., 2008; Niu and O'Hara, 2009; Niu et al., 2013).

Because the inherited zircons in QL09-01 completely covers the range defined by all the samples, it is possible that QL09-01 alone serves as the crustal endmember which can impart its inherited zircons to the derivative melt. We also conducted modelling using 800 Ma QL09-01 as crustal endmember. It gives similar results (60%–80%) (blue dash line in Fig. 8A). This again demonstrates that 797 Ma QL09-01 itself is the hybrid of mantle materials and the ancient basement. Therefore, the continental basement is involved directly or indirectly and the modelling and explanation are independent of which crustal endmembers we choose.

Samples QL09-02 and QL09-07 are distinct from others in terms of less radiogenic Nd and Hf isotopes (Fig. 8A) and obvious depleted HREEs (Fig. 5) indicative of the presence of garnet as a residual phase in the source region (Defant and Drummond, 1990; Atherton and Petford, 1993; Wolf and Wyllie, 1994; Hou et al., 2012; Wang et al., 2013). Due to the prominent negative $\varepsilon_{Nd}(450)$ and $\varepsilon_{Hf}(450)$ (−12, −12, Table 4), the source rocks of these samples must be largely of existing crustal origin. Note that 797 Ma QL09-01 has similar isotopes (Fig. 8) to those of QL09-02, contain Grt and present partial melting texture (Fig. 2) and that QL09-02 has the same inherited zircon distribution as QL09-01 and some ages matching the age of QL09-01. These indicate that QL09-02/07 is mostly the reworking products of 797 Ma intrusions presented by QL09-01. The more felsic composition of QL09-01 than

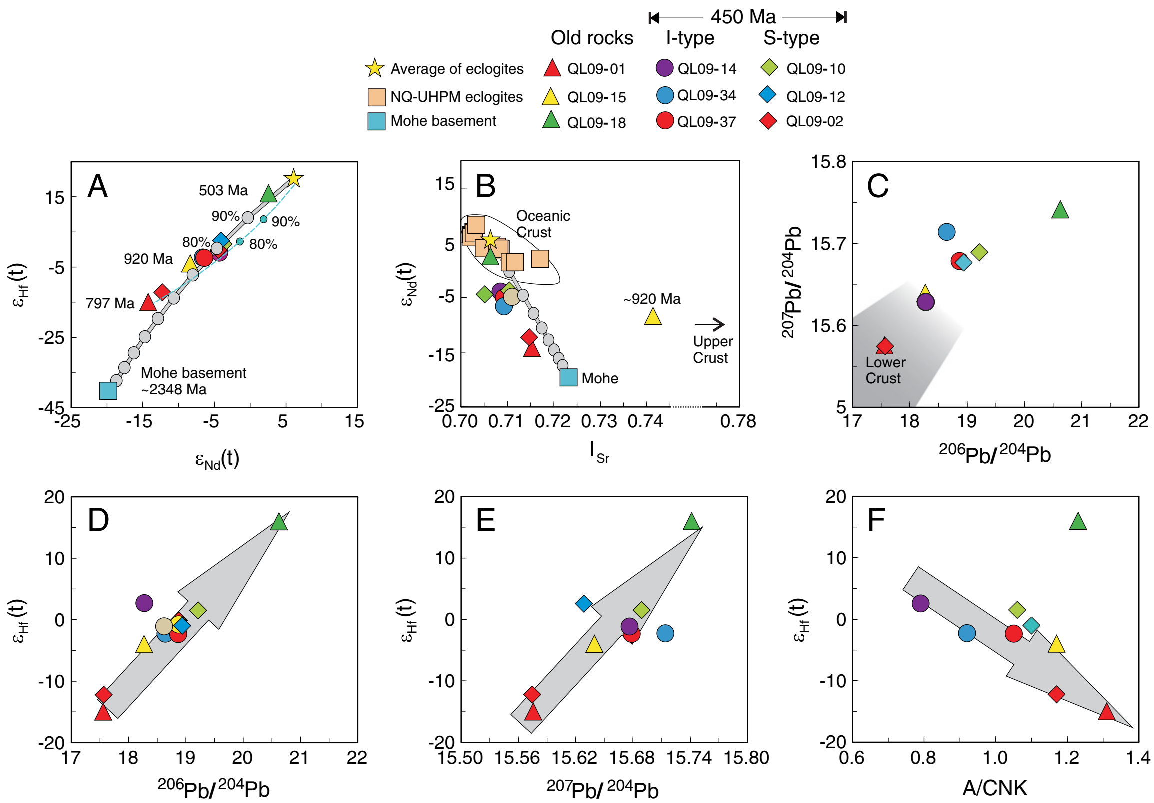

Fig. 8. Isotope plots with all the samples (including 923 Ma, 797 Ma, 503 Ma and 450 Ma) age corrected to ~450 Ma, showing significant correlations among these samples. QL09-02 has similar isotopes to 797 Ma QL09-01. The 503 Ma granite has similar isotopes to eclogites in NQ-UHPM based on the current available data for eclogites. The ~450 Ma granitoids are plotted on apparent 'mixing' trend (thick line in A) between eclogites (Qilian Ocean) and 2348–2470 Ma Mohe basement. Blue dash line in A is modelling using younger crustal endmember QL09-01 (797 Ma, this study). Sr and Nd isotope data for eclogites are from Zhang et al. (2008). Hf isotope data for eclogites are simply adopted global MORB composition (Workman and Hart, 2005). Hf isotope data for Mohe basement are from Li et al. (2007). Sr–Nd isotope data for Mohe basement are from Chen et al. (2007b).

QL09-02 indicates that QL09-01 may not be the immediate source and the mantle input in QL09-02 is also inevitable as evidenced by its slightly higher $\varepsilon_{Nd}(t)$ and $\varepsilon_{Hf}(t)$ (Fig. 8).

To conclude, both I-type and S-type granitoids contain significant mantle derived materials despite the obvious crustal contributions. Therefore, they represent a crustal growth event at ~450 Ma. This study is not the only example of 'S-type' granitoids representing crustal growth. Similar samples in South China (R.X. Wu et al., 2006) also represent the crust growth although these rocks were explained as the fast recycling of the sediments of juvenile crust.

5.3.2. Implications of tectonic context

The eclogites of MORB protolith in the NQ-UHPM belt (Yang et al., 2002; 2006; Zhang et al., 2008) and the mafic volcanism of MORB affinity in the Lajishan ophiolite (Hou et al., 2005) suggest the presence of ocean basin located between the QDB and the QB (Yang et al., 2002, 2006). The granitoids in the QB and NQ-UHPM indicate the northward subduction underneath the QB. In the NQ-UHPM, eclogite facies metamorphism happened at 461–497 Ma (Song et al., 2003a; Zhang et al., 2011) which means the collision happened shortly after. The coesite-bearing zircons in the pelitic gneisses indicate that continental material underthrust to depth of 100–200 km at 420–430 Ma (Song et al., 2005, 2009). These two time slots constrain that the collision must have happened in between. However, the precise timing remains unclear.

As emphasized above, these granitoids are both S-type and I-type intrusions. The inherited zircons of varying age (Figs. 7 and 9) indicate the very heterogeneous source. Considering the tectonic background, the most likely tectonic setting is the transition time between subduction and collision, e.g. the onset of collision, where the oceanic crust subducting together with the continental masses including the adjacent continental arcs/crust fragments as well as terrigenous sediments (Tatsumi, 2006). These subducted more silicic components and possibly the lower crust material all contributes to the crustal proportions in the 450 Ma granitoids. Varying extents of melting of the crustal rocks which are genetically derived from the same source at different times will give the 'apparent mixing' trend and the observed compositional variability of the granitoids. The dominant S-type granitoids thereafter (this study; Wu et al., 2002) are the products in response to the collision. The onset of the collision at ~450 Ma is also consistent with the exhumation at ~420–430 Ma (Song et al., 2005, 2009) which is normally 20–25 Myrs after the onset of continental collision for the old and strong subducting oceanic slab due to the slab break-off (van Hunen and Allen, 2011).

5.3.3. Melting of subducted oceanic crust

It has been demonstrated that partial melting of the last fragments of subducted ocean crust in the collision zone is necessary and possible (Mo et al., 2008; Niu and O'Hara, 2009; Huang et al., 2014). The hydrous basaltic (oceanic crust) and granitic (crustal lithologies) solidus are <650 °C at amphibole-facies (<40 km) (see Fig. 7 in Mo et al., 2008). This temperature can be easily achieved by the last fragments of oceanic crust because: (1) the arc crust lithosphere is hot; and (2) the convergence rate is significantly reduced. Petrological estimates of P–T conditions in the lowermost crust in arcs are generally high (800–1000 °C) (Peacock, 2003). Specifically, in the NQ-UHPM belt, the granulite-facies metamorphic rocks record 873–948 °C at 2.0 Ga and amphibolite facies metamorphic rocks record 660–695 °C at 0.7–0.9 Ga (Song et al., 2003b). Nevertheless, when the collision initiates, the convergence rate would be significantly reduced at least by 50% (Royden and Husson, 2009), which allows the last part of subducted ocean crust to

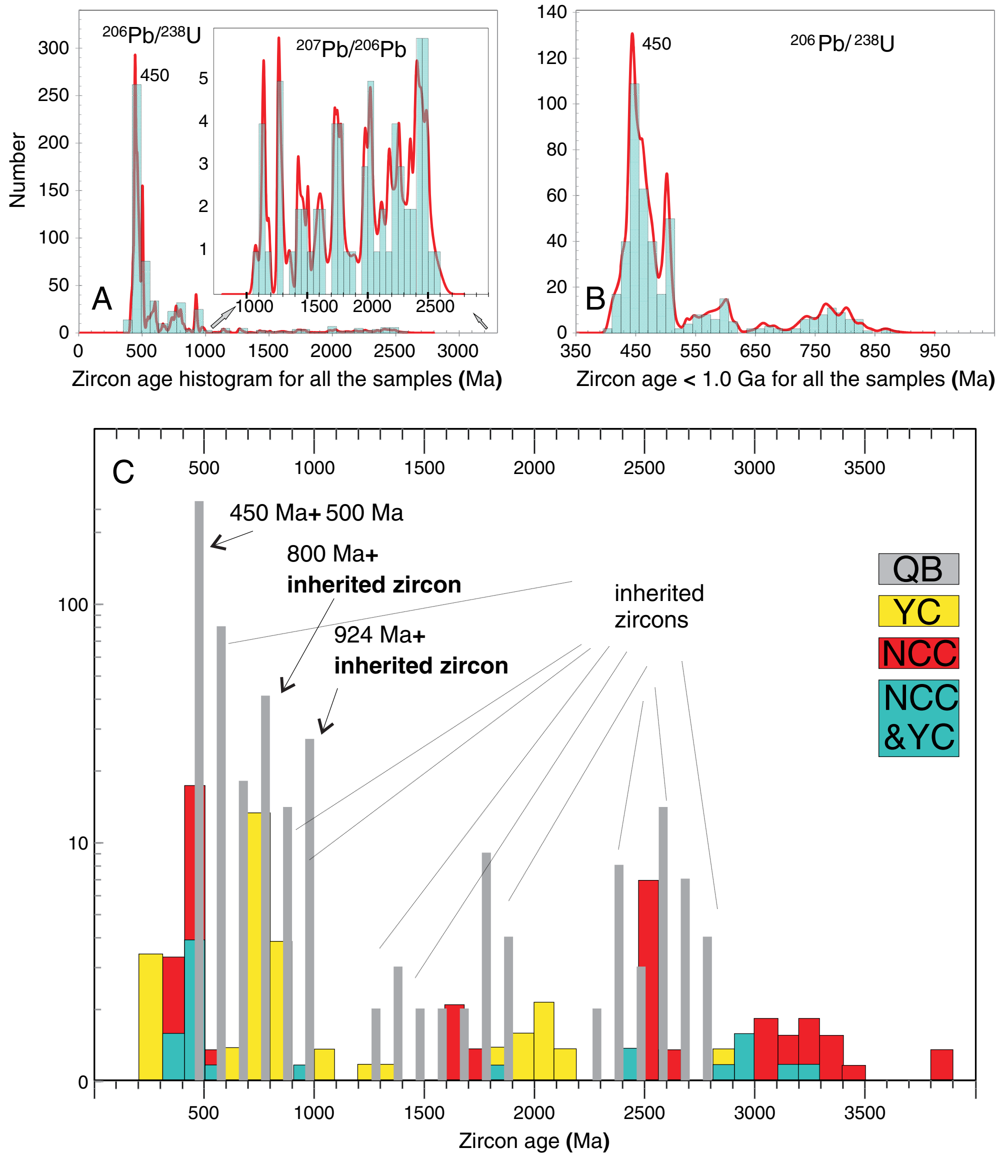

Fig. 9. The histogram of all the zircon ages ($^{206}Pb/^{238}U$ for ages < 1.0 Ga and $^{207}Pb/^{206}Pb$ for ages > 1.0 Ga). (A) Emphasizes the inherited ages > 1.0 Ga. (B) Emphasizes the inherited ages between 700 Ma and 500 Ma. (C) Comparison between North China Craton (NCC), Yangtze Craton (YC) (modified after Grimmer et al., 2003) and Qilian Block (QB) (this study).

have longer time to be heated up. All these demonstrate that arc crust lithosphere overlying above the mantle wedge during subduction then followed by collision is hot enough to reach ~800 °C at 40 km depth, therefore sufficient to heat up the subducting slab to its hydrous solidus of 650 °C at amphibole-facies (see Fig. 7 in Mo et al., 2008). Partial melting at amphibole-facies is not only supported by thermal permissions but also required by the trace elements as the majority of the samples have flat HREE patterns without the garnet signature (Fig. 5), indicating garnet is not a stable phase (<40 km, Mo et al, 2008; Huang et al, 2014).

5.4. Tectonic evolution

The NQ-UHPM, located south to the QB, is a better studied continental subduction complex with subducted/exhumed oceanic and continental crustal rocks. It is reasonable to suspect that there was a cold and fast previous subducting oceanic lithosphere to drag down the buoyant continental materials. The basaltic rocks and MORB protolith of eclogites in the NQ-UHPM record two episodes of seafloor spreading: 877–750 Ma (Yang et al., 2006; Zhang et al., 2011) and 550–500 Ma (Hou et al., 2005; Song et al., 2013). If these two periods refer to the same ocean basin spreading (Fig. 10A), the ocean must have existed for more than 370 Ma. As no ocean crust >200 Ma has survived from recycling (Niu et al., 2003), the subduction should have initiated at 677 Ma at the latest. The problem with this model is the lack of the geological record regarded to either the long lasting subduction-related arc magmatism after 677 Ma prior to 550 Ma or the formation of ocean crust at ocean ridges between 877–750 Ma and 550–550 Ma. Song et al. (2013) suggest that the inherited age of 710 Ma in the eclogite (Zhang et al., 2007) in the NQOB is regarded as the seafloor spreading. We partly agree but consider that it more likely records the earliest back-arc basin opening between QB and Alashan Block. The back-arc spreading at ~710 Ma is possible as back-arc basin extension can be shortly after the initiation of cold and fast subduction within 1 Ma (Martinez and Taylor, 2006) due to the extensive mantle wedge convection resulting from steep subduction which is comparable to the modern Mariana subduction zone. Mantle-derived 503 Ma granite might be the product in the back-arc setting. Also the back–arc spreading since 710 Ma can explain the quiescence of magmatism after 710 Ma and before 550 Ma. Importantly, the abundant concordant ages younger than 450 Ma (Figs. 7 and 9) could be the xenocrysts and compensate some unexposed or unsampled magmatic events during this quiescence period. These inherited ages could refer to either the oceanic crust

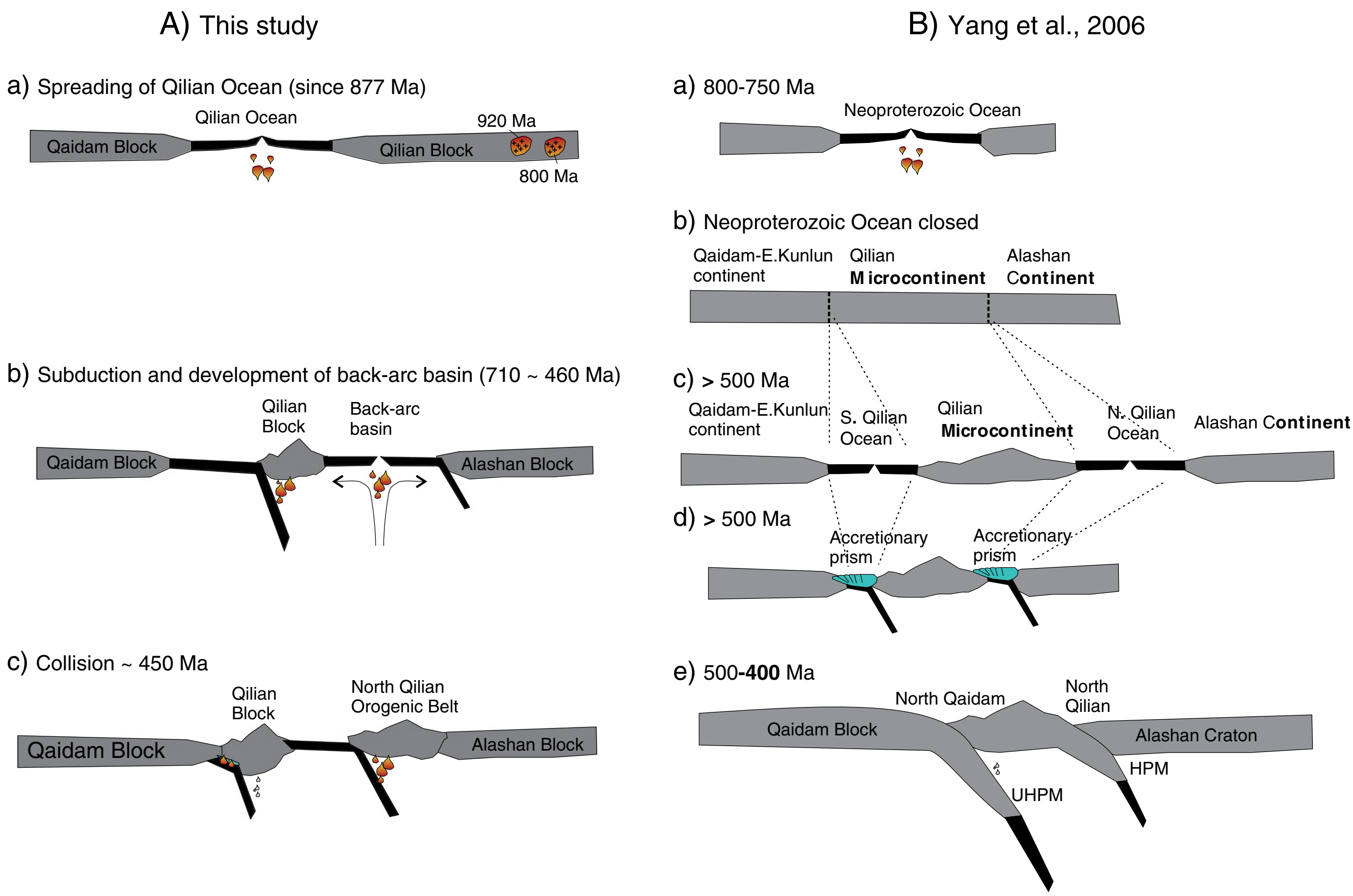

Fig. 10. Comparison of two models proposed in this study and by Yang et al. (2006), respectively. (A, this study) Cartoons showing the Qilian Ocean floor spreading between Qaidam Block and Qilian Block during the Proterozoic time (a) (877 Ma—the protolith age of eclogites in NQ-UHPM, Zhang et al., 2011), initiation of subduction and related back-arc extension (b), and the syncollisional magmatism at ~450 Ma (c). (B, Yang et al., 2006) Cartoons showing the Neoproterozoic Ocean opened and closed. Two independent Qilian oceans opened and closed during Palaeozoic time. See details in Yang et al. (2006).

formation or the subduction-related arc magmatism. In either way, they record the magmatic events. The 450 Ma magmatism is genuinely low temperature hydrous partial melting (<650 °C), therefore, it has well preserved these xenocrystal zircons. Note that our model is different from the one proposed by Song et al. (2013, 2014). We suggest that the Palaeo-Qilian Ocean located between the Qaidam Block and the Qilian Block (Fig. 10A) and the whole NQOB area was the back-arc, while they think that the Palaeo-Qilian Ocean located in the NQOB area. In our model, closure of the back-arc basin resulted in the subduction complex in the NQOB and probably has led to the secondary back-arc basin opening further north. The ~450 Ma granitoids are the products in response to the closure of the Qilian Ocean and the onset of the Qilian–Qaidam continental collision.

Alternatively, 877–750 Ma (Yang et al., 2006; Zhang et al., 2011) and 550–500 Ma (Song et al., 2013) could record oceanic crust of two different ocean basins, e.g. Neoproterozoic Ocean and Qilian Ocean, respectively (Fig. 10B) (Yang et al., 2006). The NQOB and NQ-UHPM are two independent tectonic units due to the paired subduction at the same time around >500–400 Ma (Fig. 10B) (Yang et al., 2006). This model may explain the lack of direct geological record between 877–750 Ma and 550–500 Ma. But the NQOB is a cold subduction zone (Song et al., 2007; Zhang et al., 2007) which requires the old oceanic lithosphere. In Yang's model (Yang et al., 2006), the 550–550 Ma ocean basin lived only for ~50 Ma, which is not old enough to induce the cold subduction. We suggest that our model is more reasonable, but still requires more geological evidence.

5.5. Nature of the Qilian Block

Some people consider ~920 Ma intrusions/gneisses are the basement of the Qilian Block (Zhang et al., 2003; Tung et al., 2007a, 2008). The Palaeoproterozoic and Archaean basement have to some extent been overlooked. In our study, all the inherited zircons >1.0 Ga defined a Discordia with an Archaean intercept of 2712 Ma (the final panel in Fig. 7) which is also seen in the individual sample, e.g. QL09-01 and QL09-02 (Fig. 7). These clearly confirm the existence of Archaean basement. Especially, the isotope modelling (Fig. 8) emphasizes the important role of Archaean basement in the ~450 Ma magmatism. The Qilian Block must once be a microcontinent during the assembling and the breaking-up of supercontinent and experienced multiple reworking processes later on. The magmatism of ~920 Ma and ~800 Ma was previously interpreted to be related to the Rodinia assembly (Guo et al., 1999; Wan et al., 2001, 2001b; Zhang et al., 2003; Tseng et al., 2006; Song et al., 2010b, 2013) and break-up (Zhang et al., 2003; Li et al., 2008; Song et al., 2010b), respectively. Based on our data, we can only say that 924 Ma and 797 Ma magmatic episodes are respectively crustal growth and crustal reworking processes. It has been debated that the basement of the Qilian Block has a closer link to Yangtze Craton (YC) over North China Craton (NCC) (Tung et al., 2007a and references therein) because of none magmatism during 0.6–1.6 Ga, especially 0.8–0.9 Ga in NCC (Fig. 9C, modified after Grimmer et al., 2003). Probably the most obvious conclusion from Fig. 9C is that the distribution of magmatism in the QB matches neither NCC nor YC. Based on Fig. 9, from 1.6 Ga to Archaean, the QB is comparable to both NCC and YC or maybe more closer to NCC. During 0.6–1.6 Ga, the QB and YC experienced coherent history. It might be arbitrary to say that the QB has YC affinity only because of the 0.8–0.9 Ga magmatism, especially the new finding of the ~0.9 Ga continental rifting magmatism in the NCC (Peng et al., 2011a, 2011b) which could be related to the 924 Ma in this study.

Supplementary data to this article can be found online at http://dx.doi.org/10.1016/j.gr.2014.02.010.

Acknowledgement

Hui thanks Xiaohong Xia, Pengyuan Guo, Piaoer Fu and Shuo Ding in the field. Hui thanks Lei Wu for assisting trace element analysis and Li Su, Shuijiong Wang for assisting zircon dating analysis. Discussion with Mark Allen, Pierre Bouihol, Vali Memeti, Shuguang Song, Jeroen van Hunen, and Shuijiong Wang was useful. Thanks to Shuguang Song and another anonymous reviewer whose comments and suggestions have helped improve this paper significantly. Further thanks are owed to Editor Zeming Zhang for editorial effort. The research was supported by the Chinese NSFC grants (91014003, 41130314). Hui was supported by Durham University Doctoral scholarship and China Scholarship Council.

References

Atherton, M.P., Petford, N., 1993. Generation of sodium-rich magmas from newly underplated basaltic crust. Nature 362, 144–146.
Chen, N.S., Wang, X.Y., Zhang, H.F., 2007a. Components and metamorphism of the basements of the Qaidam and Oulongbuluke micro-continental blocks, and a tentative interpretation of paleocontinental evolution in NW-Central China. Earth Science Frontiers 14, 43–55.
Chen, N.S., Wang, X.Y., Zhang, H.F., Sun, M., Li, X.Y., Chen, Q., 2007b. Geochemistry and Nd–Sr–Pb isotopic compositions of granitoids from Qaidam and Oulongbuluke micro-blocks, NW China constraints on basement nature and tectonic affinity. Journal of Earth Science 32, 7–21.
Chen, N.S., Xia, X.P., Li, X.Y., Sun, M., 2007c. Timing of magmatism of the gneissic–granite plutons along north Qaidam margin and implications for Precambrian crustal accretions: zircon U–Pb dating and Hf isotope evidences. Acta Petrologica Sinica 23, 501–512 (in Chinese with English abstract).
Chen, D., Liu, L., Sun, Y., Liou, J., 2009a. Geochemistry and zircon U–Pb dating and its implications of the Yukahe HP/UHP terrane, the North Qaidam, NW China. Journal of Asian Earth Sciences 35, 259–272.
Chen, N., Gong, S., Sun, M., Li, X., Xia, X., Wang, Q., Wu, F., Xu, P., 2009b. Precambrian evolution of the Quanji Block, northeastern margin of Tibet: insights from zircon U–Pb and Lu–Hf isotope compositions. Journal of Asian Earth Sciences 35, 367–376.
Chen, X.H., Yin, A., George, G., Li, L., Jiang, R.B., 2011. Chemical geodynamics of granitic magmatism in the basement of the eastern Qaidam basin, Northern Qinghai–Tibet Plateau. Acta Geologica Sinica 85 (157), 171 (in Chinese with English abstract).
Defant, M.J., Drummond, M.S., 1990. Derivation of some modern arc magmas by melting of young subducted lithosphere. Nature 347, 662–665.
Flagler, P.A., Spray, J.G., 1991. Generation of plagiogranite by amphibolite anatexis in oceanic shear zones. Geology 19, 70–73.
Floyd, P.A., Yaliniz, M.K., Goncuoglu, M.C., 1998. Geochemistry and petrogenesis of intrusive and extrusive ophiolitic plagiogranites, Central Anatolian Crystalline Complex, Turkey. Lithos 42, 225–241.
Gehrels, G.E., Yin, A., Wang, X.F., 2003. Magmatic history of the northeastern Tibetan Plateau. Journal of Geophysical Research 108 (B9), 2423.
Gehrels, G., Kapp, P., DeCelles, P., Pullen, A., Blakey, R., Weislogel, A., Ding, L., Guynn, J., Martin, A., McQuarrie, N., 2011. Detrital zircon geochronology of pre-Tertiary strata in the Tibetan–Himalayan orogen. Tectonics 30, TC5016.
Grimmer, J.C., Ratschbacher, L., McWilliams, M., Franz, L., Gaitzsch, I., Tichomirowa, M., Hacker, B.R., Zhang, Y., 2003. When did the ultrahigh-pressure rocks reach the surface? A $^{207}Pb/^{206}Pb$ zircon, $^{40}Ar/^{39}Ar$ white mica, Si-in-white mica, single-grain provenance study of Dabie Shan synorogenic foreland sediments. Chemical Geology 197, 87–110.
Guo, J.J., Zhao, F.Q., 2000. New chronological evidence of the age of Huangyuan in the eastern segment of mid-Qilian massif and its geological significance. Regional Geology of China 19, 26–31 (in Chinese with English Abstract).
Guo, J.J., Zhao, F.Q., Li, H.K., 1999. Jinningian collisional granite belt in the eastern sector of the central Qilian massif and its implication. Acta Geoscientia Sinica 20, 10–15 (in Chinese with English abstract).
Han, B.F., Wang, S.-G., Jahn, B.-M., Hong, D.W., Kagami, H., Sun, Y.L., 1997. Depleted-mantle source for the Ulungur River A-type granites from North Xinjiang, China: geochemistry and Nd–Sr isotopic evidence, and implications for Phanerozoic crustal growth. Chemical Geology 138, 135–159.
Hou, Q.Y., Zhang, H.F., Zhang, B.R., Zhao, Z.D., Zhu, Y.H., 2005. Characteristics and tectonic affinity of Laji Shan Paleo-Mantle in Qilian orogenic belt: a geochemical study of basalts. Journal of China University of Geosciences 30, 61–70 (in Chinese with English abstract).
Hou, Z.-Q., Zheng, Y.-C., Zeng, L.-S., Gao, L.-E., Huang, K.-X., Li, W., Li, Q.-Y., Fu, Q., Liang, W., Sun, Q.-Z., 2012. Eocene–Oligocene granitoids in southern Tibet: constraints on crustal anatexis and tectonic evolution of the Himalayan orogen. Earth and Planetary Science Letters 349–350, 38–52.
Huang, H., Niu, Y., Nowell, G., Zhao, Z., Yu, X., Zhu, D., Mo, X., Ding, S., 2014. Geochemical constraints on the petrogenesis of granitoids in the East Kunlun Orogenic belt, northern Tibetan Plateau: implications for the continental crust growth through syncollisional felsic magmatism. Chemical Geology 370, 1–18.
Irvine, T.N., Baragar, W.R.A., 1971. A guide to the chemical classification of the common volcanic rocks. Canadian Journal of Earth Sciences 8, 523–548.
Kay, R., Senechal, R., 1976. Rare earth geochemistry of the Troodos ophiolite complex. Journal of Geophysical Research 81, 964–970.
Li, X.Y., Chen, N.S., Xia, X.P., Sun, M., Xu, P., Wang, Q.Y., Wang, X.Y., 2007. Constraints on the timing of the early-Paleoproterozoic magmatism and crustal evolution of the Oulongbuluke microcontinent: U–Pb and Lu–Hf isotope systematics of zircons from Mohe granite pluton. Acta Petrologica Sinica 23, 513–522 (In Chinese with English abstract).
Li, Z.X., Bogdanova, S.V., Collins, A.S., Davidson, A., De Waele, B., Ernst, R.E., Fitzsimons, I.C. W., Fuck, R.A., Gladkochub, D.P., Jacobs, J., Karlstrom, K.E., Lu, S., Natapov, L.M., Pease, V., Pisarevsky, S.A., Thrane, K., Vernikovsky, V., 2008. Assembly, configuration, and break-up history of Rodinia: a synthesis. Precambrian Research 160, 179–210.
Liu, Y.S., Hu, Z.C., Gao, S., Gunther, D., Xu, J., Gao, C.G., Chen, H.H., 2008. In situ analysis of major and trace elements of anhydrous minerals by LA-ICP-MS without applying an internal standard. Chemical Geology 257 (1–2), 34–43.
Martinez, F., Taylor, B., 2006. Modes of crustal accretion in back-arc basins: inferences from the Lau Basin. Geophysical Monograph Series 166, 5–30.
Mo, X.X., Niu, Y.L., Dong, G.C., Zhao, Z.D., Hou, Z.Q., Su, Z., Ke, S., 2008. Contribution of syncollisional felsic magmatism to continental crust growth: a case study of the Paleogene Linzizong volcanic succession in southern Tibet. Chemical Geology 250, 49–67.
Niu, Y.L., O'Hara, M.J., 2003. Origin of ocean island basalts: a new perspective from petrology, geochemistry, and mineral physics considerations. Journal of Geophysical Research 108.
Niu, Y.L., O'Hara, M.J., 2009. MORB mantle hosts the missing Eu (Sr, Nb, Ta and Ti) in the continental crust: new perspectives on crustal growth, crust–mantle differentiation and chemical structure of oceanic upper mantle. Lithos 112, 1–17.
Niu, Y.L., O'Hara, M.J., Pearce, J.A., 2003. Initiation of subduction zones as a consequence of lateral compositional buoyancy contrast within the lithosphere: a petrological perspective. Journal of Petrology 44 (5), 851–866.
Niu, Y.L., Zhao, Z.D., Zhu, D.C., Mo, X.X., 2013. Continental collision zones are primary sites for net continental crust growth—a testable hypothesis. Earth-Science Reviews 127, 96–110.
Nowell, G.M., Kempton, P.D., Noble, S.R., Fitton, J.G., Sauders, A.D., Mahoney, J.J., Taylor, R. N., 1998. High precision Hf isotope measurements of MORB and OIB by thermal ionisation mass spectrometry: insights into the depleted mantle. Chemical Geology 149, 211–233.
Nowell, G.M., Pearson, D.G., Ottley, C.J., Schweiters, J., Dowall, D., 2003. Long-term performance characteristics of a plasma ionisation multi-collector mass spectrometer (PIMMS): the thermofinnigan neptune. Plasma Source Mass Spectrometry: Applications and Emerging Technologies. Cambridge: Royal Society of Chemistry 307–320.
Pan, G.T., Ding, J., Yao, D.S.W., L. Q., 2004. Geological Map of the Qinghai–Xizang (Tibet) Plateau and Adjacent Areas. Chengdu Cartographic Publishing House.
Peacock, S.M., 2003. Thermal structure and metamorphic evolution of subducting slabs. Geophysical Monograph—American Geophysical Union 138, 7–22.
Peng, P., Bleeker, W., Ernst, R.E., Söderlund, U., McNicoll, V., 2011a. U–Pb baddeleyite ages, distribution and geochemistry of 925 Ma mafic dykes and 900 Ma sills in the North China Craton: Evidence for a neoproterozoic mantle plume. Lithos 127, 210–221.
Peng, P., Zhai, M.-G., Li, Q., Wu, F., Hou, Q., Li, Z., Li, T., Zhang, Y., 2011b. Neoproterozoic (900 Ma) Sariwon sills in North Korea: Geochronology, geochemistry and implications for the evolution of the south-eastern margin of the North China Craton. Gondwana Research 20, 243–254.
Qinghai Geological Survey Institute, 2006. 1:250, 000 regional geological survey digital report of Xining and Menyuan In Chinese.
Rollinson, H., 2009. New models for the genesis of plagiogranites in the Oman ophiolite. Lithos 112, 603–614.
Royden, L.H., Husson, L., 2009. Subduction with variations in slab buoyancy: models and application to the Banda and Apennine systems. Subduction Zone Geodynamics 35–45.
Shi, R.D., Yang, J., Wu, C.l, IIzuka, T., Hirata, T., 2004. Island Arc volcanic rocks in North Qaidam UHP metamorphic belt. Acta Geologica Sinica 78 (52), 64 (in Chinese with English abstract).
Song, S.G., Yang, J.S., Liou, J.G., Wu, C.L., Shi, R.D., Xu, Z.Q., 2003a. Petrology, geochemistry and isotopic ages of eclogites from the Dulan UHPM Terrane, the North Qaidam, NW China. Lithos 70, 195–211.
Song, S.G., Yang, J.S., Xu, Z.Q., Liou, J.G., Shi, R.D., 2003b. Metamorphic evolution of the coesite-bearing ultrahigh-pressure terrane in the North Qaidam, Northern Tibet, NW China. Journal of Metamorphic Geology 21, 631–644.
Song, S., Zhang, L., Niu, Y., Su, L., Jian, P., Liu, D., 2005. Geochronology of diamond-bearing zircons from garnet peridotite in the North Qaidam UHPM belt, Northern Tibetan Plateau: a record of complex histories from oceanic lithosphere subduction to continental collision. Earth and Planetary Science Letters 234, 99–118.
Song, S., Zhang, L., Niu, Y., Su, L., Song, B., Liu, D., 2006. Evolution from oceanic subduction to continental collision: a case study from the Northern Tibetan Plateau based on geochemical and geochronological data. Journal of Petrology 47, 435–455.

Song, S.G., Zhang, L.F., Niu, Y., Wei, C.J., Liou, J.G., Shu, G.M., 2007. Eclogite and carpholite-bearing metasedimentary rocks in the North Qilian suture zone, NW China: implications for Early Palaeozoic cold oceanic subduction and water transport into mantle. Journal of Metamorphic Geology 25, 547–563.
Song, S.G., Niu, Y.L., Zhang, L.F., Zhang, G.B., 2009. Time constraints on orogenesis from oceanic subduction to continental subduction, collision, and exhumation: an example from North Qilian and North Qaidam HP–UHP belts. Acta Petrologica Sinica 25, 2067–2077.
Song, S., Niu, Y.L., Wei, C.J., Ji, J.Q., Su, L., 2010a. Metamorphism, anatexis, zircon ages and tectonic evolution of the Gongshan Block in the northern Indochina continent—an eastern extension of Lhasa Block. Lithos 120, 3–4.
Song, S., Su, L., Li, X.-h, Zhang, G., Niu, Y., Zhang, L., 2010b. Tracing the 850-Ma continental flood basalts from a piece of subducted continental crust in the North Qaidam UHPM belt, NW China. Precambrian Research 183 (805), 816.
Song, S., Su, L., Li, X.H., Niu, Y.L., Zhang, L.F., 2012. Grenville-age orogenesis in the Qaidam–Qilian block: the link between South China and Tarim. Precambrian Research 220, 9–22.
Song, S., Niu, Y., Su, L., Xia, X., 2013. Tectonics of the North Qilian orogen, NW China. Gondwana Research 23, 1378–1401.
Song, S.G., Niu, Y.L., Su, L., Zhang, C., Zhang, L.F., 2014. Continental orogenesis from seafloor subduction, continent collision/subduction, to orogen collapse, and orogen recycling: the example of the North Qaidam UHPM belt, NW China. Earth-Science Reviews 129, 59–84.
Spulber, S.D., Rutherford, M.J., 1983. The origin of rhyolite and plagiogranite in oceanic crust: an experimental study. Journal of Petrology 24, 1–25.
Sun, S.S., McDonough, W.F., 1989. Chemical and isotopic systematics of oceanic basalts: implications for mantle composition and processes. Geological Society, London, Special Publications 42, 313–345.
Tatsumi, Y., 2006. High-Mg andesites in the Setouchi volcanic belt, southwestern Japan: analogy to Archean magmatism and continental crust formation? Annual Review of Earth and Planetary Sciences 34, 467–499.
Thirlwall, M.F., 1991. Long-term reproducibility of multi-collector Sr and Nd isotope ratio analysis. Chemical Geology: Isotope Geoscience section 94, 85–104.
Tseng, C.-Y., Yang, H.-Y., Yusheng, W., Dunyi, L., Wen, D.-J., Lin, T.-C., Tung, K.-A., 2006. Finding of Neoproterozoic (775 Ma) magmatism recorded in metamorphic complexes from the North Qilian orogen: evidence from SHRIMP zircon U–Pb dating. Chinese Science Bulletin 51, 963–970.
Tseng, C.Y., Yang, H.J., Yang, H.Y., Liu, D.Y., Wu, C.L., Cheng, C.K., Chen, C.H., Ker, C.M., 2009. Continuity of the North Qilian and North Qinling Orogenic blets, Central Orogenic System of China: Evidence from newly discovered Palaeozoic adakitic rocks. Gondwana Research 16, 285–293.
Tung, K.A., Yang, H.J., Yang, H.Y., Liu, D.Y., Zhang, J.X., Wan, Y.S., Tseng, C.Y., 2007a. SHRIMP U–Pb geochronology of the zircons from the Precambrian basement of the Qilian Block and its geological significances. Chinese Science Bulletin 52, 2687–2701.
Tung, K.A., Yang, H.Y., Liu, D., Zhang, J.X., Tseng, C.Y., Wan, Y.S., 2007b. SHRIMP U–Pb geochronology of the detrital zircons from the Longshoushan Group and its tectonic significance. Chinese Science Bulletin 52, 1414–1425.
Tung, K.A., Yang, H.R., Yang, H.Y., Liu, D.Y., Zhang, J.X., Wan, Y.S., Zeng, J.Y., Zhuang, Y.R., 2008. Qilian Neoproterozoic granitoids SHRIMP zircon U–Pb geochronology, elemental and Sr–Nd isotope geochemistry. Bulletin of Mineralogy, Petrology and Geochemistry 27, 106–108.
van Hunen, J., Allen, M.B., 2011. Continental collision and slab break-off: a comparison of 3-D numerical models with observations. Earth and Planetary Science Letters 302, 27–37.
Wan, Y.S., Xu, Z.Q., Yang, J.S., Zhang, J.X., 2001. Ages and compositions of the Precambrian high-grade basement of the Qilian Terrane and its adjacent areas. Acta Geologica Sinica 75 (375), 384 (English Edition).
Wang, S.-J., Li, S.-G., Chen, L.-J., He, Y.-S., An, S.-C., Shen, J., 2013. Geochronology and geochemistry of leucosomes in the North Dabie Terrane, East China: implication for post-UHPM crustal melting during exhumation. Contributions to Mineralogy and Petrology 165 (5), 1009–1029.
Whitney, D.L., Evans, B.W., 2010. Abbreviations for names of rock-forming minerals. American Mineralogist 95, 185–187.
Wolf, M.B., Wyllie, P.J., 1994. Dehydration-melting of amphibolite at 10 kbar: the effects of temperature and time. Contributions to Mineralogy and Petrology 115, 369–383.
Workman, R.K., Hart, S.R., 2005. Major and trace element composition of the depleted MORB mantle (DMM). Earth and Planetary Science Letters 231, 53–72.
Wu, C.L., Yang, J.S., Ireland, T., Wooden, J.L., Li, H.B., Wan, Y.S., Shi, R.D., 2001. Zircon SHRIMP ages of Aolaoshan granite from the south margin of Qilianshan and its geological significance. Acta Petrologica Sinica 17, 215–221.
Wu, C.L., Yang, J.S., Wooden, J., Liou, J., Li, H., Shi, R., Meng, F., Persing, H., Meibom, A., 2002. Zircon SHRIMP dating of granite from Qaidamshan, NW China. Chinese Science Bulletin 47, 418–422.
Wu, C.L., Yao, S.Z., Zeng, L.S., Chen, S.Y., Li, H.B., Qi, X.X., Joseph, L.W., Mazdab, F.K., 2006a. Double subduction of the Early Paleozoic North Qilian oceanic plate: evidence from granites in the central segment of North Qilian, NW China. Geology in China 33, 1197–1208 (in Chinese with English abstract).
Wu, R.X., Zheng, Y.F., Wu, Y.B., Zhao, Z.F., Zhang, S.B., Liu, X.M., Wu, F.Y., 2006b. Reworking of juvenile crust: element and isotope evidence from Neoproterozoic granodiorite in South China. Precambrian Research 146, 179–212.
Wu, C.L., Gao, Y.H., Wu, S., Chen, Q., Wooden, J.L., Mazadab, F.K., Mattinson, C., 2007. Zircon SHRIMP U–Pb dating of granites from the Da Qaidam area in the north margin of Qaidam Basin, NW China. Acta Petrologica Sinica 23, 1861–1875 (in Chinese with English abstract).
Wu, C.L., Xu, X.Y., Gao, Q.M., Li, X.M., Lei, M., Gao, Y.H., Ronald, B.F., Joseph, L.W., 2010. Early Palaezoic granitoid magmatism and tectonic evolution in North Qilian, NW China. Acta Petrologica Sinica 26 (1027), 1044 (in Chinese with English abstract).
Xia, X., Song, S., 2010. Forming age and tectono-petrogenises of the Jiugequan ophiolite in the North Qilian Mountain, NW China. Chinese Science Bulletin 55, 1899–1907.
Xiao, W.J., Windley, B.F., Yong, Y., Zhen, Y., Chao, Y., Liu, C.Z., Li, J., 2009. Early Paleozoic to Devonian multiple-accretionary model for the Qilian Shan, NW China. Journal of Asian Earth Sciences 35, 323–333.
Xu, Z.Q., Xu, H.F., Zhang, J.X., Li, H.B., Zhu, Z.Z., Qu, J.C., Chen, D.N., Chen, J.L., Yang, K.C., 1994. The Zoulang Nanshan Caledonian subduction complex in the Northern Qilian Mountains and its dynamics1. Acta Geologica Sinica 7 (225), 241 (English Edition).
Xu, W.C., Zhang, H.F., Liu, X.M., 2007. U–Pb zircon dating constraints on formation time of Qilian high-grade metamorphic rock and its tectonic implications. Chinese Science Bulletin 52, 531–538.
Yang, J.S., Xu, Z.Q., Zhang, J.X., Song, S.G., Wu, C.L., Shi, R.D., Li, H.B., Maurice, B., 2002. Early Palaeozoic North Qaidam UHP metamorphic belt on the north-eastern Tibetan plateau and a paired subduction model. Terra Nova 14, 397–404.
Yang, J.S., Wu, C.L., Zhang, J., Shi, R., Meng, F., Wooden, J., Yang, H.-Y., 2006. Protolith of eclogites in the north Qaidam and Altun UHP terrane, NW China: earlier oceanic crust? Journal of Asian Earth Sciences 28, 185–204.
Yin, A., Harrison, T.M., 2000. Geologic evolution of the Himalayan–Tibetan Orogen. Annual Review of Earth and Planetary Sciences 28, 211–280.
Yong, Y., Xiao, W.J., Yuan, C., Yan, Z., Li, J.L., 2008. Geochronology and geochemistry of Paleozoic granitic plutons from the eastern Central Qilian and their tectonic implications. Acta Petrologica Sinica 24, 855–866 (in Chinese with English Abstract).
Zhang, J.X., Wan, Y.S., Meng, F.C., Yang, J.S., Xu, Z.Q., 2003. Geochemistry, Sm–Nd and U–Pb isotope study of gneisses (schists) enclosing eclogites in the North Qaidam Mountains—deeply subducted Precambrian metamorphic basement. Acta Petrologica Sinica 19, 443–451 (in Chinese with English abstract).
Zhang, J.X., Yang, J.S., Meng, F.C., Wan, Y.S., Li, H.M., Wu, C.L., 2006. U–Pb isotopic studies of eclogites and their host gneisses in the Xitieshan area of the North Qaidam Mountains, western China: new evidence for an early Paleozoic HP–UHP metamorphic belt. Journal of Asian Earth Sciences 28, 143–150.
Zhang, J.X., Meng, F.C., Wan, Y.S., 2007. A cold Early Palaeozoic subduction zone in the North Qilian Mountains, NW China: petrological and U–Pb geochronological constraints. Journal of Metamorphic Geology 25, 285–304.
Zhang, G., Song, S., Zhang, L., Niu, Y., 2008. The subducted oceanic crust within continental-type UHP metamorphic belt in the North Qaidam, NW China: evidence from petrology, geochemistry and geochronology. Lithos 104, 99–118.
Zhang, C., Zhang, L., Roermund, H.V., Song, S., Zhang, G., 2011. Petrology and SHRIMP U–Pb dating of Xitieshan eclogite, North Qaidam UHP metamorphic belt, NW China. Journal of Asian Earth Sciences 42, 752–767.
Zheng, Y.F., Xiao, W.J., Zhao, G.C., 2013. Introduction to tectonics of China. Gondwana Research 23 (4), 1189–1206.